高等学校化学学报
CHEMICAL JOURNAL OF CHINESE UNIVERSITIES
综合评述

聚集诱导发光镧系配合物

张凯为，秦安军
（华南理工大学发光材料与器件全国重点实验室，广东省分子聚集发光重点实验室，广州 510640）

摘要 聚集诱导发光(AIE)镧系配合物结合了镧系离子独特的光物理性质与AIE特性，在多个领域具有应用价值．然而，迄今尚未有文献对该领域的研究进展进行系统梳理．本文基于镧系中心数目总结了AIE镧系配合物的研究进展，并阐述了其作用机制及在刺激响应和生物成像等领域的应用．最后，简要探讨了AIE镧系配合物当前面临的挑战及未来研究方向．

关键词 聚集诱导发光；镧系配合物；天线效应；分子内运动受限
中图分类号 O614 **文献标志码** A doi：10.7503/cjcu20260013

Lanthanide Complexes with Aggregation-induced Emission

ZHANG Kaiwei，QIN Anjun*
（*State Key Laboratory of Luminescent Materials and Devices*，*Guangdong Provincial Key Laboratory of Luminescence from Molecular Aggregates*，*South China University of Technology*，*Guangzhou* 510640，*China*）

Abstract Lanthanide complexes with aggregation-induced emission（AIE）integrate the unique photo-physical properties of lanthanide ions and the AIE features，making them applicable in diverse areas. However，the progress in this area has been rarely reviewed. Herein，we summarize the advance of AIE lanthanide complexes based on the number of lanthanide centers they contain，along with the mechanism and applications in the fields of stimulus-responsive and biological imaging. Meanwhile，the current challenges and the future research directions in this area are also briefly discussed.

Keywords Aggregation-induced emission；Lanthanide complex；Antenna effect；Restriction of intramolecular motion

1 Introduction

Aggregation-induced emission（AIE），a scientific concept coined by Tang *et al.*[1] in 2001，has revolutionized the design and application of luminescent materials. The AIE stands in sharp contrast to the well-documented aggregation-caused quenching（ACQ）effect，where conventional fluorophores suffer from luminescence attenuation or quenching in aggregate states due to the intermolecular π-π stacking. However，the AIE luminogens（AIEgens）exhibit weak or no emission in dilute solution but undergo significant luminescence enhancement upon aggregation，unlocking new possibilities for solid-state luminescent devices，bioimaging probes，and chemical sensors that rely on condensed-phase emission[2—5].

The fundamental origin of AIE in most systems can be attributed to two mechanisms：restriction of

收稿日期：2026-01-04. 网络首发日期：2026-02-10.
联系人简介：秦安军，男，博士，教授，主要从事三键单体的高分子合成化学和有机聚合物功能材料方面的研究．
E-mail: msqinaj@scut.edu.cn
基金项目：广东省分子聚集发光重点实验室项目(批准号：2023B1212060003)资助．
Supported by the Fund of Guangdong Provincial Key Laboratory of Luminescence from Molecular Aggregates(No.2023B1212060003).

intramolecular rotation (RIR) and restriction of intramolecular vibration (RIV) (Fig.1)[6,7]. These two mechanisms can be unified as the restriction of intramolecular motion (RIM). Among them, the RIR is the most extensively studied mechanism, referring to the suppression of free rotation or twisting of flexible molecular moieties in aggregate states. In dilute solutions, these motions dissipate excited-state energy *via* non-radiative pathways, leading to a weak luminescence; whereas, the aggregation imposes steric hindrance and intermolecular interactions that "lock" these motions, redirecting energy toward radiative decay. RIV complements RIR by confining high-frequency intramolecular vibration in aggregates, further reducing non-radiative energy loss and reinforcing emission intensity. It is worth noting that in certain specific circumstances, these two mechanisms may operate simultaneously. Together, these mechanisms provide a unified framework for understanding AIE in diverse molecular systems.

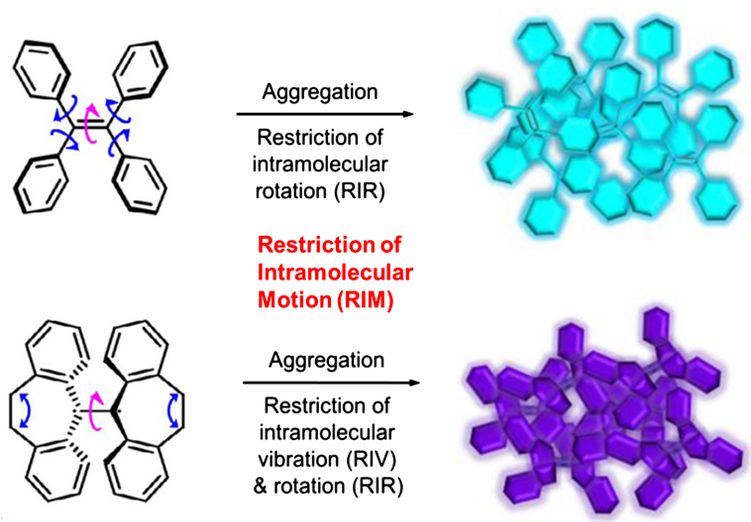

Fig. 1 Schematic illustration of the restriction of intramolecular motions mechanisms in AIEgens[7]

Copyright 2015, American Chemical Society.

To date, besides the organic AIEgens, the AIE organometallic complexes have been well studied[8—11]. The majority of these type AIEgens are constructed using transition metals. While these AIEgens have demonstrated versatility in optoelectronics and sensing applications, their emission spectra are typically broad (full width at half maximum, FWHM>50 nm) due to metal-to-ligand charge transfer (MLCT) or intra-ligand charge transfer (ILCT) transitions. This spectral broadening limits their further applicability in scenarios requiring high color purity, multiplexed detection, or precise spectral resolution. In contrast, lanthanide complexes offer unique advantages that address these limitations, leveraging their intrinsic photo-physical properties derived from 4*f* electron configurations[12,13]. These properties include narrow, line-like emission bands from forbidden *f*-*f* transitions with a FWHM less than 10 nm, large Stokes shifts that avoid self-quenching, long luminescence lifetimes on the microsecond to millisecond scale that enable time-gated detection to eliminate background interference, and excellent photo-stability under prolonged excitation. However, lanthanide ions inherently suffer from small molar absorption cross-sections due to the shielding effect of outer 5*s* and 5*p* orbitals on the 4*f* orbitals, resulting in inefficient direct excitation[14]. To overcome this limitation, organic ligands are essential as "antennas" to mediate the antenna effect. The ligand first absorbs photon energy, undergoes intersystem crossing from the singlet excited state to the triplet excited state, and then transfers the energy to the excited state of Ln^{3+}, thereby sensitizing efficient luminescence. This ligand-mediated energy transfer strategy effectively addresses the intrinsic limitation of lanthanide ions, rendering the lanthanide complexes the most widely applied form of lanthanide-based materials. Lanthanide complexes have been

widely used as fluorescence probes, scintillators and anti-counterfeiting materials[15—17]. This wide applicability stems from the synergistic effect of the energy transfer efficiency of the antenna effect and the inherent optical physical advantages of lanthanide ions, which makes lanthanide complexes the cornerstone of research on functional luminescent materials.

Among the lanthanide complexes, AIE lanthanide complexes are particularly attractive. They overcome the quenching limitation of traditional lanthanide complexes caused by aggregation. By restricting intramolecular motion and inhibiting non-radiative decay, they exhibit enhanced luminescence properties in the aggregate state. By combining the environmental responsiveness of AIE feature with the inherent advantages of luminescent lanthanide complexes, these complexes can achieve stimulus-responsive luminescence and extend to solid-state systems, aggregation-based sensors, and *in vivo* imaging, *etc*. Their tunability of structure further supports the customization of performance. Meanwhile, the research on them meets the demand for multifunctional materials with both high efficiency and responsiveness, and advances the basic understanding of the structure-property relationship in luminescence aggregation systems.

Significant progress has been made in the field of AIE lanthanide complexes. However, the existing reviews only focus on their synthesis methods or isolated functional applications, and there is no comprehensive summary of the AIE properties of rare earth complexes[18,19]. Herein, we systematically summarize the research progress of AIE luminescent lanthanide complexes classified by the number of Ln centers because they directly modulates the coordination environment intermolecular interaction modes and ligand-to-metal energy transfer efficiency factors. This classification strategy overcomes the limitations of traditional ligand-based categorization by intuitively elucidating how an increasing number of Ln centers regulates aggregation-induced motion restriction, thereby offering a more comprehensive understanding of the structure-property relationships in AIE lanthanide complexes. Furthermore, it generalizes the intrinsic mechanisms underlying the AIE effect associated with different Ln center configurations and establishes a robust foundation for the rational design and development of high-performance AIE lanthanide materials.

2 AIE Lanthanide Complexes

2.1 Mononuclear Systems

2.1.1 Complexes with AIE-active Ligands A natural and straightforward strategy for designing AIE-active lanthanide complexes lies in integrating well-established AIE moieties into the ligand framework. This approach avoids the need for *de novo* design of novel luminescent ligands, leveraging the intrinsic aggregation-responsive emission properties of existing AIEgens to ensure compatibility with lanthanide coordination and efficient energy transfer. Among classic AIEgens, tetraphenylethylene (TPE) emerges as a preferred candidate due to its robust AIE feature, excellent structural tunability, and facile functionalization to incorporate coordination-competent groups that enable stable binding to lanthanide ions while retaining AIE characteristics[20—24].

A compelling illustration of this TPE-based design strategy is demonstrated in the work by Deng *et al.*, who developed a lanthanide complex (complex **1**) integrating the ACQ ligand $hfac^-$ and AIE ligand TPE-TPY as dual sensitizers to achieve stable Eu^{3+} luminescence across a broad concentration range [Fig. 2(A)][20]. The sensitizers are stepwise activated: $hfac^-$ dominates at low concentrations ($\leqslant 10^{-5}$ mol/L), both act in the 10^{-4}—10^{-3} mol/L range, and TPE-TPY becomes the sole donor above 10^{-3} mol/L *via* aggregation. The AIE mechanism of TPE-TPY could be ascribed to the RIR: dilute solutions exhibit weak emission due to energy dissipation from rapid rotations of twisted aromatic rings, while aggregation constrains these rotations, suppressing non-radiative decay and enhancing energy transfer to Eu^{3+}. Enabled by shielding effect of Ln^{3+}

ions and inner *f-f* transitions, the complex also allows real-time concentration monitoring *via* the linear correlation between maximum excitation wavelength and lg*M* (R^2=0.97), offering a promising strategy for smart bioprobes and solid-state emitters.

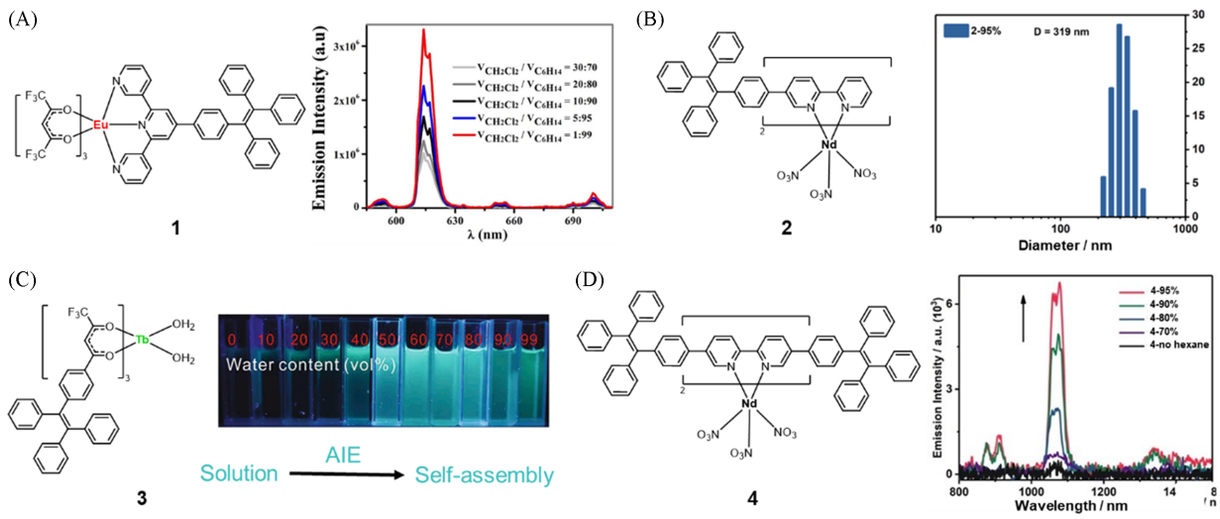

Fig. 2 Molecular structure of complex 1 and photoluminescence(PL) spectra of complex 1 in dichloromethane with different volume fractions of *n*-hexane(A)[20], molecular structure of complex 2 and DLS of complex 2 in *n*-hexane/chloroform mixtures with the *n*-hexane content of 95%(B)[22], molecular structure of complex 3 and fluorescent photographs of complex 3(C)[23] and molecular structure of complex 4 and PL spectra of complex 4 in chloroform with different volume fractions of *n*-hexane(D)[22]

(A) Copyright 2015, Springer Nature; (B, D) Copyright 2021, John Wiley and Sons; (C) Copyright 2021, Elsevier Ltd.

Beyond this dual-sensitizer design, Tang *et al.* explored an alternative TPE-modification strategy for lanthanide complexes by grafting it onto a pyridine-azole ligand rather than the terpyridine described earlier, and two complexes denoted as Ln(hfac)$_3$(TPE-tz)(Ln=Eu, Dy) were synthesized[21]. The Eu complex exhibits AIE feature as aggregation restricts TPE intramolecular rotation and promotes ligand-to-Eu^{3+} energy transfer. In contrast, the Dy complex shows weak luminescence due to mismatched energy levels but displays field-induced single-molecule magnet behavior. This work demonstrates an alternative TPE-modification strategy for multifunctional lanthanide complexes.

Building on the foundational insights from single-TPE-unit complexes, Zeng *et al.* next explored the impact of two TPE units in AIE-active ligands TPE-BPY for Nd(III)-based lanthanide complex **2**, aiming to enhance conformational rigidity and ligand-to-metal energy transfer efficiency [Fig. 2(B)][22]. The two TPE moieties work synergistically to strengthen molecular conformational rigidity upon aggregation, which suppresses non-radiative transitions, optimizes energy matching with Nd^{3+} ions and the antenna effect, and facilitates ligand-to-metal energy transfer *via* triplet ligand-to-metal charge transfer (^{3}LMCT). Additionally, twisted intramolecular charge transfer (TICT) under aggregation condition shifts the excitation window toward lower energy, endowing the complexes with aggregation-induced phosphorescence enhancement (AIPE) activity, improved near-infrared (NIR) phosphorescence intensity, and prolonged luminescence lifetimes, marking a clear performance upgrade compared to their single-TPE counterparts.

To further validate the structure-performance correlation, that increasing TPE units amplifies luminescent advantages, Tang *et al.*[23,24] extended the design to complexes incorporating three TPE units in their AIE-active ligands. They developed Tb^{3+} complex(complex **3**) containing three TPE moieties in its β-diketone ligands and two coordinated water molecules [Fig. 2(C)][23]. The complex spontaneously self-assembles into

spherical nanoparticles in organic/water mixed systems. The self-assembled nanostructures possess a rigid shell-like architecture, which restricts intramolecular rotation and vibration of the TPE moieties, locks non-radiative decay pathways, and activates radiative decay. The coordination of Tb^{3+} with the ligands further stabilizes the aggregate structure, while the presence of anthrax spore biomarker 2,6-dipicolinic acid strengthens Tb^{3+}-specific luminescence *via* enhanced coordination and reduced water-induced quenching, enabling ratiometric sensing based on the modulated emission of the aggregate complex.

After investigating complexes with two TPE-functionalized ligands, Zeng *et al.*[22] further explored the impact of increasing TPE moiety number on the aggregation-related luminescent properties of lanthanide complexes. They developed complex **4** with a ten-coordinate structure, where the central Nd^{3+} ion is chelated by two TPE_2-BPY ligands and three nitrate ions[Fig.2(D)]. When equipped with four TPE units, the molecular conformational rigidity is strengthened more significantly owing to the enhanced steric hindrance and intermolecular interactions, leading to more efficient inhibition of non-radiative dissipation. This structural optimization also boosts the ligand-to-Nd^{3+} energy transfer efficiency, enabling the corresponding complexes to exhibit superior NIR luminescent property. Specifically, the crystal form of the four-TPE complex shows a PL lifetime of 9.69 μs at 1064 nm, one of the longest reported for C-H-containing Nd^{3+}-based complexes, along with higher NIR emission intensity and more prominent AIPE activity than that with two TPE units.

Beyond TPE-based systems, a class of lanthanide complexes has been constructed using ligands that inherently possess aggregation-related emission characteristics, which enriches the structural diversity of AIE-active lanthanide materials and offers alternative strategies for tailoring luminescent behavior through ligand intrinsic properties. To validate this expanded ligand design strategy, Tang *et al.*[25] synthesized a Eu^{3+} complex(complex **5**)[Fig.3(A)], where the central Eu^{3+} ion is coordinated with β-diketone ligands(HTHA) featuring extended conjugated alkylcarbazole moieties and inherent AIE properties[Fig.3(B)]. Complex **5** undergoes a J-aggregation-driven self-assembly to form uniform spherical nanoparticles(**5 NPs**) in ethanol/water mixed systems. The spatial confinement effect within the **5 NPs** not only reinforces the AIE performance of the ligand by further constraining molecular motions but also provides effective shielding for Eu^{3+} ions against solvent-induced quenching. In comparison to the discrete complex **5**, the **5 NPs** exhibit remarkably enhanced luminescent performance: the absolute PL quantum yield(Φ_F) increases from 12.84% to 21.25%, and the emission lifetime extends from 269 to 402 μs. Such enhancement is attributed to the synergistic effects of AIE-mediated emission amplification and the inhibition of non-radiative decay processes caused by spatial limitations, highlighting the critical role of supramolecular assembly in optimizing the photo-physical properties of lanthanide complexes.

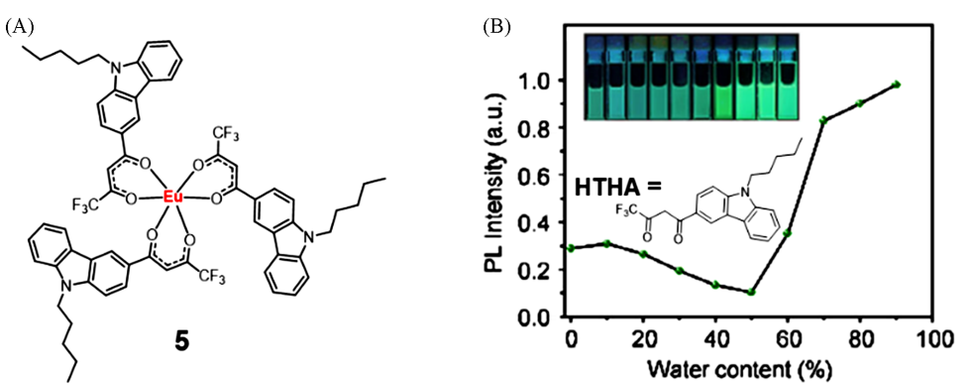

Fig. 3 Molecular structure of complex 5(A) and PL intensity profile of ligand HTHA at 470 nm in ethanol with different volume fractions of water and fluorescent photographs of HTHA(B)[25]

2.1.2 Complexes Without AIE-active Ligands Apart from the well-established paradigm of lanthanide complexes bearing inherently AIE-active ligands where ligand-based AIE feature is retained or amplified following metal coordination and supramolecular assembly, a compelling extension emerges. This extension involves complexes that exhibit AIE properties even when their free ligands lack such activity. This phenomenon arises from metal-ligand coordination-driven structural and photo-physical modifications, including rigid coordination frameworks, RIM of ligand moieties, and unique intermolecular interactions during aggregation. These factors collectively suppress non-radiative decay and activate efficient radiative emission, bridging ligand-derived and complex-induced AIE strategies while expanding the scope of viable ligands for luminescent lanthanide materials.

Among the diverse lanthanide complexes, β-diketone-based systems stand as the most classical and extensively investigated example, owing to their strong chelating capacity and favorable triplet energy level matching with lanthanide ions[26]. These complexes leverage the efficient antenna effect of β-diketone ligands to sensitize the characteristic narrow-band *f*-*f* transition luminescence of Ln^{3+}, featuring high Φ_F, long emission lifetimes, and excellent photo-stability. Their structural tunability, hydrophobicity, or intermolecular interactions, further underpins their enduring utility as a foundational platform for designing luminescent lanthanide materials.

Yoshizawa *et al.*[27] developed complex **6** featuring a structure where the central Eu^{3+} ion is coordinated with one phenanthroline ligand and three β-diketone ligands thenoyltrifluoroacetone(tta), which exhibits high hydrophobicity with a molecular size of approximately 1.3 nm[Fig.4(A)]. In aqueous media, complex **6** is non-emissive due to vibrational quenching by water molecules but undergoes encapsulation into the hydrophobic cavities of aromatic micelles self-assembled from bent amphiphilic compounds with two pentamethylphenyl and two alkanesulfonate groups. This encapsulation induces significant luminescence enhancement as the tight hydrophobic environment restricts intramolecular rotation of the phenyl moieties in the ligands, suppressing non-radiative relaxation pathways, while the aromatic shell of the micelles effectively shields the Eu^{3+} center from water-induced quenching. The resultant host-guest nanocomposite exhibits prominent red emission with an absolute Φ_F of 48.3% and an emission lifetime of 1.05 ms in water, both significantly improved compared to the free complex. This enhancement mechanism, originating from motion restriction and environmental shielding, is analogous to aggregation-related luminescent behavior; however, it is realized through host-guest encapsulation rather than through direct aggregation of the complex itself.

Following the observation that Eu(III) complexes can achieve AIE feature *via* encapsulation by aromatic micelles, researchers further discovered that β-diketone lanthanide complexes themselves intrinsically exhibit such luminescent behavior without relying on external host matrices. For example, Zhang *et al.*[28] substituted the β-diketone ligand tta with dbm(dibenzoylmethane) and prepared complex **7**, which features ligand centers with π-π^* transition characteristics(exhibiting intense absorption peaks at 235 nm and 340 nm), and displays AIE behavior[Fig.4(A)]. In pure THF or mixed solvents with a water volume fraction (f_w) below 80%, complex **7** shows weak and stable PL due to solvent-induced quenching and unconstrained molecular motions; however, as the f_w increases to 99%(volume fraction), it undergoes pronounced aggregation, leading to a significant PL enhancement, along with a maximum Φ_F of 41.9% and prolonged PL lifetime. The AIE mechanism of complex **7** is distinct from traditional organic AIEgens: low water fractions(0—10%) initially promote vibrational coupling and solvent exchange to induce quenching, while high water fractions drive aggregation that disrupts these quenching pathways by impeding solvent exchange and electronic-vibrational decoupling, restricting intramolecular rotation/vibration of the ligand moieties and thus suppressing non-radiative decay.

Law *et al.*[29] reported an Eu(III)-based complex(complex **8**), where the ligand was replaced with

chloride-functionalized dbm (*pp*-dbm-Cl_2) [Fig. 4 (A)]. Crystallizing in the centrosymmetric space group $P2_1/n$, complex **8** adopts a bicapped trigonal prism coordination geometry, with extensive intermolecular $\pi\cdots\pi$ stacking, C—H$\cdots\pi$ interactions, and C—H$\cdots$Cl—C interactions stabilizing its crystal packing. In dilute tetrahydrofuran solutions, complex **8** shows weak luminescence due to solvent-induced quenching and unconstrained molecular motions; however, as the water fraction in mixed solvents increases to 80% and above, it undergoes aggregation to form hydrophobic nanostructures. This aggregation restricts intramolecular rotation of the phenyl moieties of ligands, suppresses non-radiative energy dissipation, and shields the Eu^{3+} center from water-induced vibrational quenching, leading to significant luminescence enhancement. Solid-state luminescence is further amplified *via* rigid molecular packing stabilized by extensive intermolecular interactions, reinforcing the AIE effect.

Moving beyond the β-diketone ligands utilized above, Yan *et al.*[30] developed the amphiphilic complex (complex **9**), which incorporates carbazole-derived ligands, and exhibits self-assembly-induced luminescence

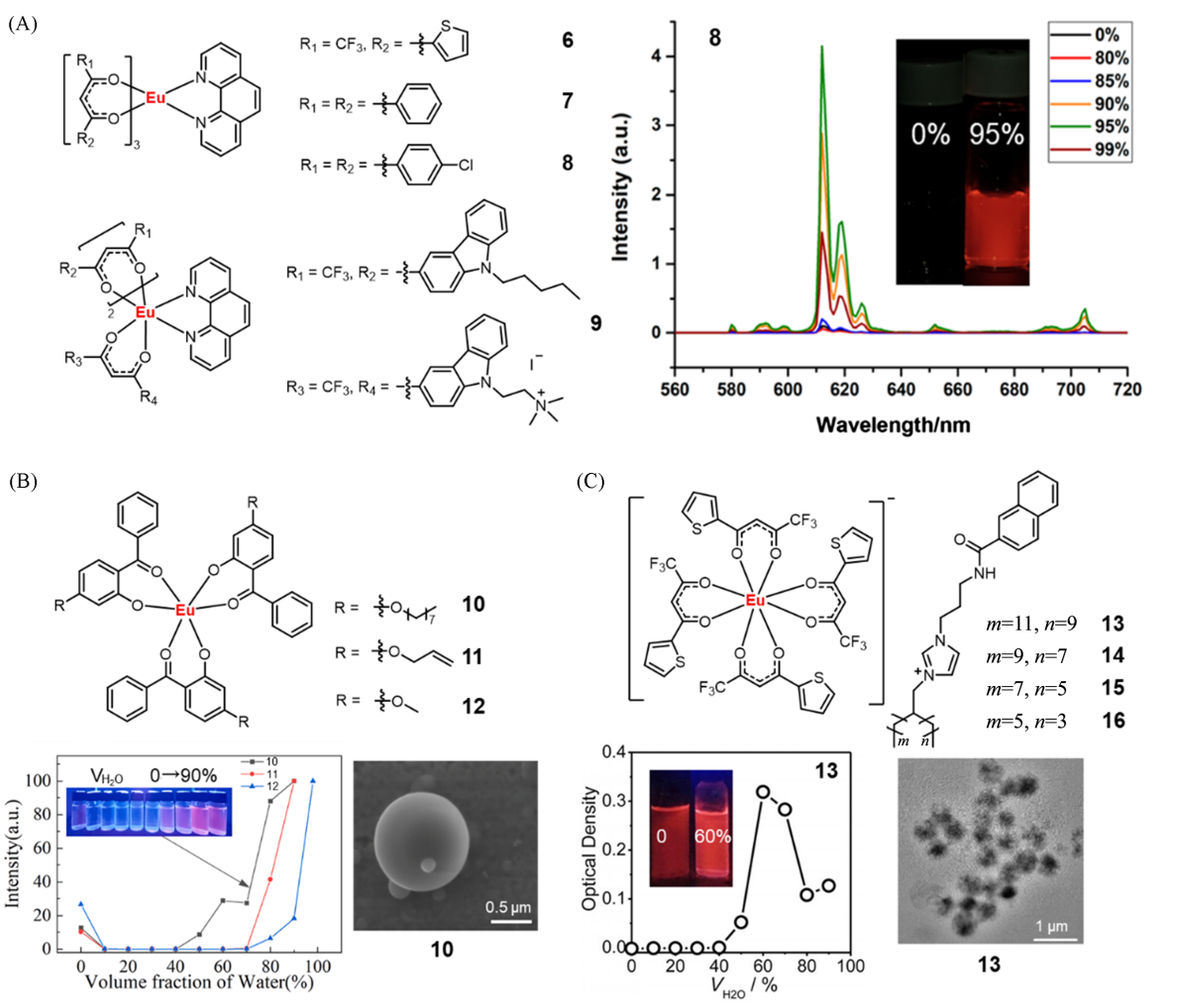

Fig. 4 Molecular structure of β-diketone complexes 6—9 and PL spectra of complex 8 in THF with different volume fraction of water(A)[29], molecular structure of complexes 10—12 and PL intensity profile of complexes 10—12 at 615 nm in acetone with different volume fractions of water, SEM image of complex 10 with the water volume fraction of 90%(B)[31], molecular structure of complexes 13—16 and optical density of complex 13 at 500 nm in ethanol with different volume fractions of water, TEM image of aggregates formed by complex 13 in ethanol/water mixtures with water volume fraction of 60%(C)[32]

(A) Copyright 2019, MDPI; (B) Copyright 2025, Elsevier Ltd.; (C) Copyright 2018, John Wiley and Sons.

(SAIL) analogous to AIE in aqueous media[Fig.4(A)]. In organic/water binary solvents, complex **9** undergoes self-assembly driven by hydrophobic interactions, hydrogen bonding, and π-π stacking when the water fraction exceeds 40%, leading to a significant luminescence enhancement. The overall Φ_F values increases from 3.4% to 24.0% and the emission lifetime is also prolonged. This SAIL phenomenon originates from two synergistic mechanisms: the self-assembly restricts intramolecular rotation/vibration of the complex, suppressing non-radiative decay, and the assembled nanostructure shields Eu^{3+} centers from water-induced quenching. The nanoparticles of complex **9** also exhibit good biocompatibility and mitochondrial targeting ability, supporting their potential in bioimaging applications.

Beyond the aforementioned lanthanide complexes adhering to the canonical structural motif of three β-diketone ligands and one phenanthroline ligand, research in this field has expanded further to explore structural variants that deviate from this general formula. A notable direction involves the development of complexes where the coordination sphere is solely composed of β-diketone ligands, without incorporating phenanthroline or analogous nitrogen-containing auxiliary ligands[31,32]. This structural adjustment not only enriches the diversity of β-diketone lanthanide complexes but also provides a platform to investigate how the absence of auxiliary ligands and the modulation of β-diketone structures influence aggregation-related luminescent behaviors, ligand-to-metal energy transfer efficiency, and overall photophysical performance.

For example, Zhao *et al.*[31] reported three Eu^{3+} complexes (**10**—**12**) with structurally similar β-diketone ligands differ only in the pendant functional groups of the ligands: octyloxyl for complex **10**, allyloxyl for complex **11**, and methoxyl for complex **12**[Fig.4(B)]. In acetone/water mixtures, all the three complexes show weak luminescence at low water fractions due to solvent quenching, but undergo self-assembly into aggregates at high water fractions (≥40% for complex **10**, ≥70% for complex **11** and **12**), leading to significant luminescence enhancement. Complex **10**, with the longest carbon chain in its ligand, displays the most prominent performance: its aggregates form smooth spherical structures, achieving a solid-state Φ_F of 21.36%. The underlying mechanism involves self-assembly-induced spatial confinement that restricts intramolecular rotation/vibration of the complexes and shields Eu^{3+} centers from water-induced quenching, while the triplet energy level of the ligand facilitates energy transfer to Eu^{3+}. Notably, the self-assembly behavior also enhances the photostability of complex **10** compared to traditional β-diketone Eu^{3+} complexes, highlighting the critical role of carbon chain length in regulating self-assembly and optimizing emission properties.

Like the previous system where alkyl chain length modulates assembly behavior, Hao *et al.*[32] developed four complexes (**13**—**16**), which are composed of tta as the chelating ligand and imidazolium cations with naphthyl groups and branched alkyl chains as counterions. The main difference among these four complexes lies in the lengths of the alkyl chains on the imidazole cations[Fig.4(C)]. In ethanol/water mixtures, complex **13** exhibits distinct assembly behavior triggered by water content when the alkyl chain of the cation is sufficiently long. Below 50% water content (volume fraction), the complex exists as discrete molecules with weak luminescence due to water-induced quenching. When water content exceeds 50%, it spontaneously assembles into solid spherical aggregates and eventually vesicles at 90% water content, with aggregate sizes decreasing from around 1000 to 100 nm as water content increases. The aggregate structure restricts intramolecular motion and effectively shields the Eu^{3+} center from vibrational quenching by water molecules, leading to enhanced characteristic Eu^{3+} emission at 612 nm, accompanied by increased Φ_F and prolonged lifetime. This emission enhancement arises from the aggregates encapsulating $Eu(tta)^{4-}$ anions, shielding Eu^{3+} centers from water-induced vibrational quenching and restricting intramolecular motions, while the naphthyl groups on the imidazolium cations exhibit ACQ effect. In contrast, complexes with shorter alkyl chains (**14**—**16**) fail to form effective aggregates, showing no luminescence enhancement and confirming the critical role of long branched

alkyl chains in driving self-assembly and optimizing emission performance.

While β-diketone ligands have established themselves as robust and versatile building blocks for AIE lanthanide complexes, their utility stems from strong chelating ability, tunable triplet energy levels, and facilitation of self-assembly-driven motion restriction. Research in this domain has further expanded to explore ligands other than β-diketones. These ligands encompass diverse coordination motifs such as pyridine-derived ones, carboxylates, or heterocyclic derivatives, and feature tailored functional groups that introduce distinct intermolecular interaction modes and aggregation behaviors. In turn, they modulate the underlying luminescence enhancement mechanisms, offering alternative pathways to achieve aggregation-related emission and advancing the design of high-performance AIE lanthanide materials with expanded application potential.

To construct novel AIE europium complexes, Zou *et al.*[33—35] made great progress in this field. They developed two pairs of dynamic chiral Eu^{3+} enantiomers, **17**(**R**) and **17**(S)[Fig. 5(A)], and **18**(**R**) and **18**(S)][Fig. 5(B)][33]. In the molecular state, these complexes exhibits negligible emission as the free rotation of phenyl ring rotors in the ligand dissipates excited-state energy *via* non-radiative transitions. However, upon aggregation, strong intermolecular hydrogen bonds and steric hindrance restrict intramolecular rotation within the aggregates, which readily closes non-radiative decay pathways and promotes efficient intersystem crossing, leading to a significant luminescence enhancement with an aggregation enhancement factor(α_{AIE}) up to 92. 54[**17**(**R**)], accompanied by excellent circularly polarized luminescence performance. Additionally, the aggregate complexes display high sensitivity toward Cu^{2+} ions. This work demonstrates that integrating molecular rotors or vibrational units into chiral ligands is a robust approach to design dynamic Eu^{3+} complexes with desirable AIE and CPL feature, providing valuable insights for multifunctional chiral

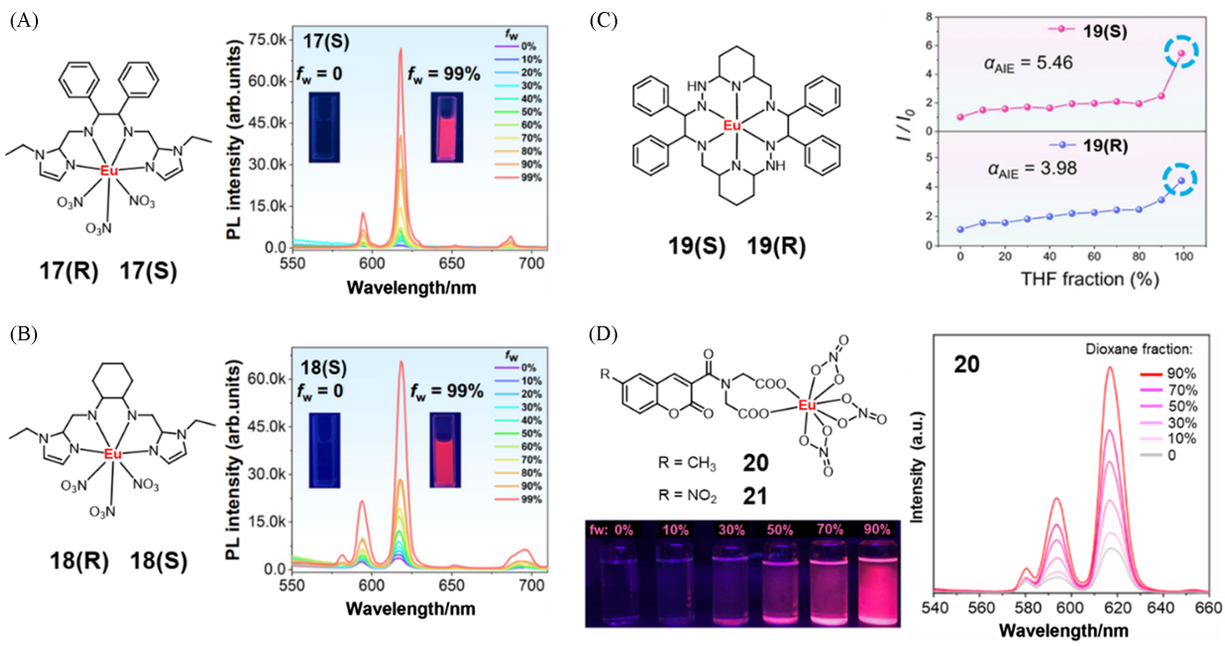

Fig. 5 Molecular structure of chiral complexes 17(R) and 17(S) and PL spectra of complex 17(S) in DMSO with different fraction of glycerin(A)[33], molecular structure of chiral complexes 18(R) and 18(S) and PL spectra of complex 18(S) in DMSO with different fraction of glycerin(B)[33], molecular structure of chiral complexes 19(R) and 19(S) and PL intensity profile of complexes 19(R) and 19(S) at 611 nm in DMSO with different fraction of THF(C)[35], and molecular structure of complexes 20 and 21, fluorescent photographs and PL spectra of complex 20 in DMF with different fraction of 1,4-dioxane(D)[36]

(A) Copyright 2024, Springer Nature; (B) Copyright 2024, Springer Nature; (C) Copyright 2025, Springer Nature; (D) Copyright 2020, John Wiley and Sons.

lanthanide-based materials. Subsequently, they discovered that these two pairs of complexes have potential applications in cell imaging and zebrafish imaging[34].

With the same synthetic strategies, Zhu *et al.*[35] developed a pair of complexes [**19**(S) and **19**(R)] using a macrocyclic cationic dimer structure with parallel-arranged molecular rotors[Fig. 5(C)]. Following a similar mechanism to prior analogs, aggregation restricts the free rotation of molecular rotors through strong π-π stacking, hydrogen bonding and steric effects, which enhance the antenna effect by promoting intersystem crossing and efficient ligand-to-Eu^{3+} energy transfer. Complex **19**(S) exhibits notable AIE feature with α_{AIE} of 5.46, alongside excellent CPL performance, achieving a luminescence asymmetry factor (g_{lum}) of 0.084 and a CPL brightness (B_{CPL}) of 612.88 $L\cdot mol^{-1}\cdot cm^{-1}$. The aggregate complex also demonstrates superior bioimaging capabilities, further validating the versatility of molecular rotor-containing chiral Eu^{3+} complexes in aggregation-enhanced luminescent and biomedical applications.

Meanwhile, Guo *et al.*[36] developed two Eu^{3+} complexes (**20** and **21**), which are constructed from coumarin-derived ligands (L^1 and L^2) with intramolecular charge transfer (ICT) effects, where L^1 carries an electron-donating group and L^2 carries an electron-withdrawing group[Fig. 5(D)]. The characteristic Eu^{3+} luminescence of two complexes is enhanced with increasing complex concentration or fraction of poor solvent in DMF-based mixed systems. The mechanism originates from strengthened intermolecular interactions upon aggregation, which restrict ligand molecular motion and reinforce the conjugated system, while the triplet energy levels of the ligands are well-matched with excited state energy levels of Eu^{3+}. This synergy promotes efficient ligand-to-metal energy transfer and suppresses non-radiative decay, leading to intensified luminescence. This work illustrates that rational design of ligands with push-pull electronic systems is a viable strategy for developing Eu^{3+} complexes with desirable AIE feature.

Notably, beyond conventional lanthanide complexes with intentional structural twisting to trigger AIE, recent studies have explored unconventional systems once unforeseen to show such behavior. This pursuit of non-traditional candidates breaks conventional design paradigm, revealing AIE feature in lanthanide complexes is more widespread than previously recognized ones. It enriches material diversity and provides a new insight for developing facile, low-cost luminescent systems for sensing, imaging and optoelectronics.

For example, Zhang *et al.*[37] developed series complexes (**22**—**24**) with decorated porphyrin ligands [Fig. 6(A)]. It is worth noting that one of the main obstacles of porphyrins is the fluorescence quenching caused by the strong intermolecular π-π interactions of its planar structure during aggregation. Therefore, to address this issue, researchers modified the porphyrins with AIEgens[38]. However, an unexpected AIE effect was observed in complex **22**. In aqueous media, protonation of the carboxyphenyl groups on the porphyrin at pH<5.0 reduces the solubility of the complex, inducing aggregation with particle sizes increasing from <5 nm to 200—300 nm as pH value decreases from 5.0 to 1.0. This aggregation restricts intramolecular motion and minimizes exposure of the Yb^{3+} center to water, suppressing vibrational quenching and extending the luminescence lifetime from 135 to 170 μs. Complex **22** displays distinct pH-sensitive NIR emission from pH 9.0 to 5.0 in aqueous solution, showing enhanced emission intensity and aggregation-induced lifetime prolongation at lower pH[Fig. 6(B)]. It has a pK_a value of —6.6, which correlates well with its wide-range pH-responsive luminescent behavior[Fig. 6(C)]. This study demonstrates that the pH value-driven aggregation phenomenon of lanthanide porphyrin complexes provides a feasible approach for designing responsive luminescent materials.

Another notable case of unexpected aggregation-related luminescent behavior in lanthanide complexes is reported by Tang *et al.*[39], who observed significant luminescence enhancement in an Eu(III) nitrate complex (**25**) *via* a distinct unconventional mechanism unrelated to traditional aggregation-induced motion

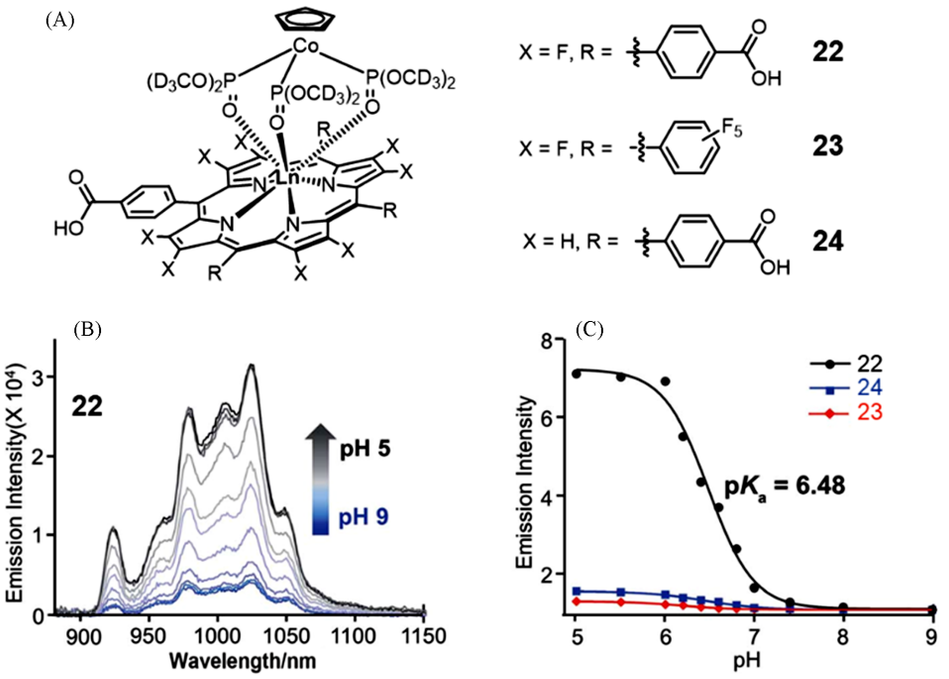

Fig. 6 Molecular structure of complexes 22—24(A), fluorescence emission spectra of complex 22 in PBS buffer(pH=5. 0—9. 0)(B), and the normalized emission intensity ratio of complexes 22—24 according to the value at pH 9. 0 *versus* the pH values in the pH range 5. 0—9. 0(C)[37]

restriction[Fig. 7(A)]. At low concentrations, the complex displays weak luminescence due to strong electronic-vibrational coupling between Eu^{3+} electronic states and high-frequency vibrational modes of coordinating solvents, which facilitates non-radiative decay. However, the complex undergoes coordination environment reorganization under two distinct conditions, both of which trigger electronic-vibrational decoupling (EVD). With increasing concentration, water molecules coordinated to the complex are replaced by nitrate ions, which are ligands with lower vibrational energies[Fig. 7(B)]. When the solvent is switched to DMF or DMF-water mixtures, coordinated water molecules are substituted by DMF molecules, which also possess lower vibrational energies[Fig. 7(C)]. This EVD mechanism suppresses non-radiative relaxation by reducing the resonance between solvent vibrational energies and Eu^{3+} energy gaps. Importantly, no colloidal or nanoparticulate aggregates were detected, even at high concentrations, which further emphasizes the unconventional nature of the

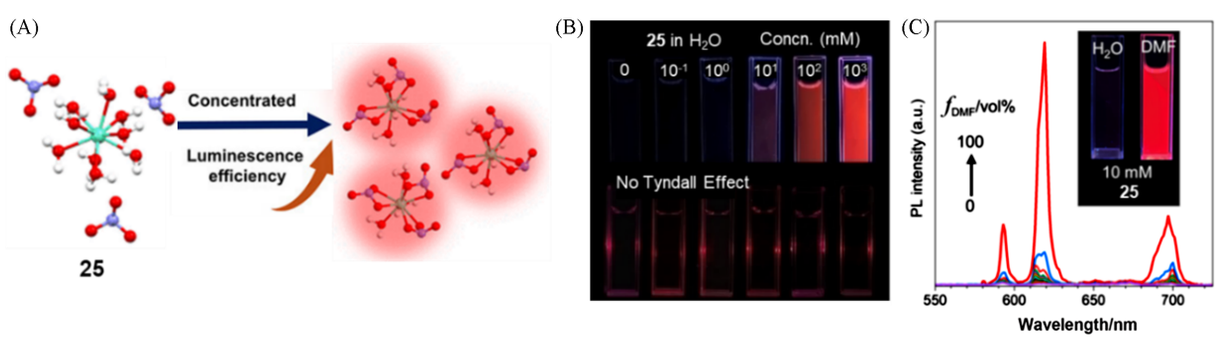

Fig. 7 Schematic diagram of the structural changes of complex 25 from low concentration to aggregated state(A), fluorescence photographs of complex 25 solutions and laser for Tyndall effect test(B) and fluorescence emission spectra of complex 25 in water with different fraction of DMF and fluorescence photograph complex 25 in water and DMF(C)[39]

luminescent behavior. This behavior is primarily rooted in EVD-driven coordination restructuring rather than traditional aggregation-induced motion restriction.

2.2 Dinuclear Systems

Apart from extensively studied mononuclear complexes, dinuclear systems have also been documented in recent studies[40—42]. In contrast to the mononuclear counterparts that rely on single metal centers for regulate luminescence, dinuclear architectures integrate two lanthanide ions linked by bridging ligands. These structures deliver enhanced structural flexibility, coordination tunability and interionic communication. Such attributes facilitate ligand-to-metal energy transfer and generate unique luminescent responses, advancing AIE performance and functional versatility.

The first AIE dinuclear complex (**26**) was developed by Yan *et al.*[40], in which two Sm^{3+} centers are coordinated by three bis-β-diketone ligands (BTPB) with four water molecules participating in coordination [Fig.8(A)]. The abundant aromatic rings of the ligand enable facile aggregation in solutions. At low concentrations, BTPB exhibits monomeric blue emission. Elevated concentration or the use of chloroform, a solvent that favors aggregation, triggers the formation of complex aggregates and gives rise to a new blue-green emission. In the aggregated complexes, partial energy transfer takes place from BTPB to Sm^{3+}. This process produces the characteristic red emission of Sm^{3+} together with ligand-derived emission. The balance between these emission enables tunable white-light output, which can be adjusted by concentration or excitation wavelength. The emission enhancement associated with aggregation arises from restricted intramolecular motion of the ligand and optimized ligand-to-metal energy transfer, which is facilitated by the well-matched triplet energy level of BTPB with the excited state of Sm^{3+} and further reinforced by the aggregate structure. This work demonstrates that rational ligand design in dinuclear triple-stranded complex **26** enables

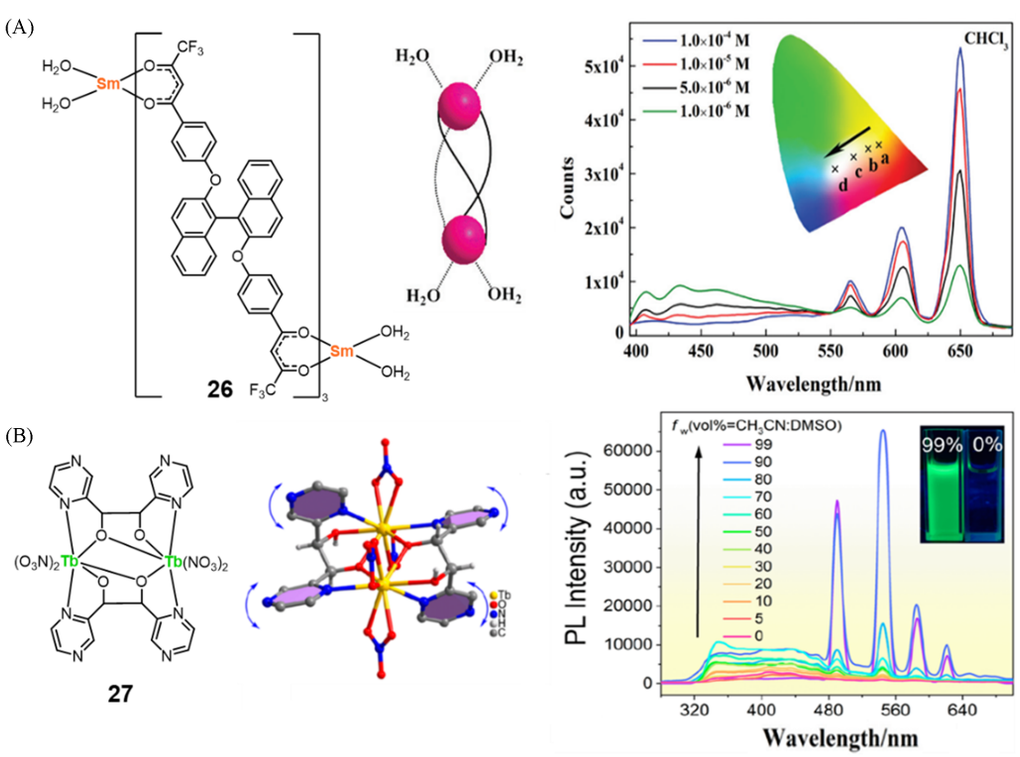

Fig. 8 Molecular structure and schematic diagram of complex 26, PL spectra of complex 26 in THF at different concentrations(A)[40] and molecular structure and structural diagram of complex 27, PL spectra of complex 27 in DMSO with different fraction of CH_3CN(B)[41]

(A) Copyright 2014, the Royal Society of Chemistry; (B) copyright 2023, American Chemical Society.

aggregation-modulated multi-color emission, with white light as one of the achievable outputs.

To extend the scope of AIE dinuclear complexes, Zou *et al.*[41] developed a Tb^{3+}-based dinuclear complex (**27**). This complex incorporates butterfly-configured pinacol ligands and exhibits AIE behavior *via* a distinct mechanism rooted in RIV[Fig. 8(B)]. In good solvents such as DMSO, the pinacol ligands undergo vigorous vibrational motion driven by steric hindrance and structural distortion. These motions dominate non-radiative decay pathways, resulting in negligible emission. In contrast, adding poor solvents like CH_3CN induces complex aggregates formation with size *ca.* 68. 42 nm. These aggregates effectively constrain the intramolecular vibrations of the pinacol ligands. This restriction suppresses non-radiative transitions, promotes intersystem crossing, and enhances the antenna effect. These effects facilitate efficient energy transfer to Tb^{3+} ions, leading to prominent characteristic emissions of Tb^{3+}. This work enriches the mechanistic diversity of aggregation-responsive lanthanide complexes. It also highlights RIV as a viable strategy for designing dynamic luminescent materials, which hold potential applications in sensing and anticounterfeiting.

2.3 Polynuclear Systems

2.3.1 Metallopolymers Beyond discrete mononuclear and dinuclear lanthanide complexes, metallopolymers integrate the structural versatility of polymers with the unique photophysical properties of lanthanides. Assembled *via* coordination between lanthanide centers and multidentate ligands, they form extended structures that surpass discrete complex limitations[43,44]. Their structural diversity enables precise regulation of aggregation behavior, intermolecular interactions and energy transfer processes. To systematically investigate their design principles and photophysical properties, the following section classifies metallopolymers by their architectural features, exploring how structural variations govern AIE mechanisms and functions.

Su *et al.*[45] developed lanthanide coordination polymers [**28**(**Ln**)] by assembling a tetrapodal TPE-derived ligand(TPE-4PO) with various Ln^{3+}(Ln=Sm, Eu, Gd, Tb, Dy). These polymers possess a hierarchically ordered structure: each TPE-4PO ligand acts as a four-connecting node[Fig. 9(A)], linking Ln^{3+} ions (10-coordinated with nitrate anions and water molecules) into one-dimensional loop-and-chain frameworks. These frameworks further assemble into two-dimensional layered structures *via* π-π interactions[Fig. 9(B)]. This backbone-integrated design grants the polymers inherent structural rigidity, a key advantage over mononuclear systems[Fig. 9(C)]. This work bridges the gap between mononuclear TPE-based complexes and AIE metallopolymers. Its skeletal design enhances structural stability and luminescent tunability, expanding the application potential of such materials in sensors, optoelectronics, and bio-probes while enriching the structural

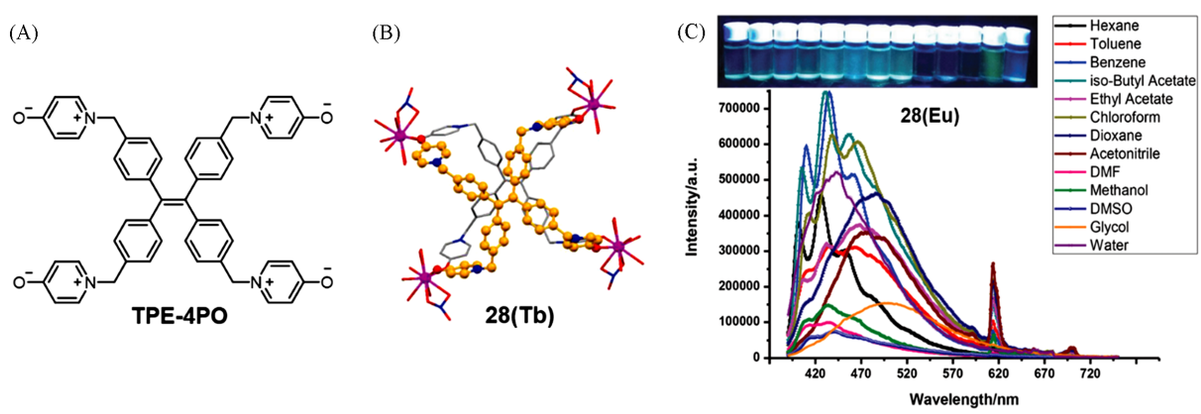

Fig. 9 Molecular structure of ligand TPE-4PO(A), the coordination environment of Tb^{3+} ions and TPE-4PO ligands in the crystal of complex 28(Tb)(B) and fluorescent photographs and PL spectra of complex 28(Eu) in various solvents(C)[45]

diversity of AIE coordination polymers.

Beyond incorporating of the TPE-based AIE unit into polymers, the metallopolymers without such AIE unit can still exhibit distinct AIE feature. This phenomenon stems from intrinsic structural features, including rigid network architectures and constrained coordination environments, which suppress non-radiative decay during aggregation. For instance, Sunkari *et al.*[46] developed a 1D Pr^{3+} coordination polymer(**29**), where nine-coordinate Pr^{3+} ions are bridged by mono- or fully deprotonated pyridine-2,6-dicarboxylate ligands($dipicH_2$), with extensive hydrogen bonding between coordinated or lattice water and carboxylate groups. The polymer emits weakly in dilute solutions. In the solid state or mixed solvents with high water content, however, it undergoes aggregation, which leads to enhanced NIR-II emission with peak at 1028 nm[Fig. 10(A)]. The mechanism of AIE involves aggregation-induced structural rigidification whereby intermolecular interactions and hydrogen bonding restrict ligand motions, suppress non-radiative decay, and optimize ligand-to-Pr^{3+} energy transfer. This study pioneers aggregation-driven NIR-II emission in lanthanide coordination polymers.

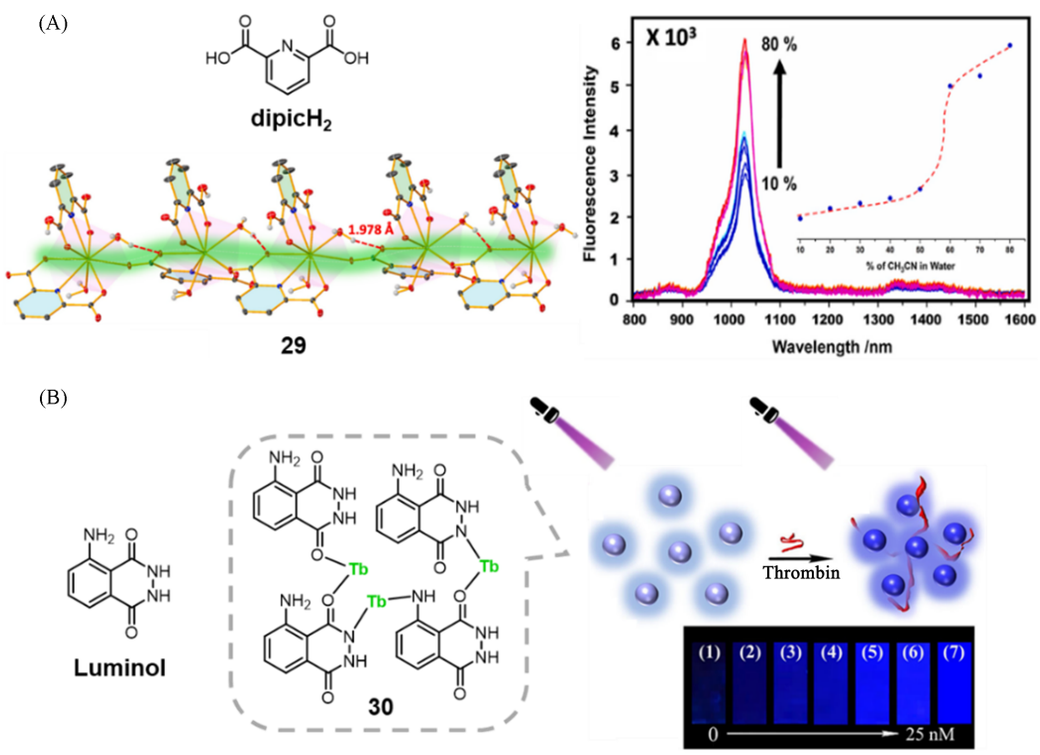

Fig. 10 Molecular structure of ligand $dipicH_2$ and crystal structure of polymer 29, PL spectra of polymer 29 in CH_3CN with different fraction of water(A)[46] and molecular structure of ligand luminol and polymer 30, fluorescent photographs of the polymer 30 dispersed in Tris buffer in the presence of various concentrations of thrombin(B)[49]

(A) Copyright 2025, Elsevier Ltd.; (B) Copyright 2019, Springer Nature.

Researchers have made significant progress in developing lanthanide coordination polymers containing luminogen with AIE properties for biosensing applications[47—49]. For example, Qiu *et al.*[49] developed a nanoparticle-based coordination polymer **30**, using luminol as the bridging ligand and Tb^{3+} as the central metal ion. This complex exhibits enhanced fluorescence upon aggregation, which is triggered by the coordination between thrombin and polymer **30**. Such aggregation increases the rigidity of the ligand linker, restricts intramolecular motions, and suppresses non-radiative decay pathways to boost the fluorescence intensity of luminol[Fig. 10(B)]. This study integrates aggregation-modulated emission into a biosensing platform for sensitive thrombin detection. It also underscores the potential of such ligand-metal complexes in biological

analysis, leveraging structure rigidification-driven luminescence enhancement.

Coordination polymers feature Ln^{3+} as integral main-chain nodes. By contrast, another class of metallopolymers has lanthanide ions coordinated to the polymer main chain. This structural transformation separates the polymer main chain from the lanthanide-containing groups. It also preserves the inherent flexibility of the main chain while enabling precise control over the coordination environment of lanthanide ions. Such a design offers distinct advantages, including enhanced processability and tunable intermolecular interactions. These merits expand the structural diversity and functional versatility of AIE lanthanide metallopolymers.

Akcelrud *et al.*[50] developed a europium-containing metallopolymer (**31**) with an alternating conjugated backbone composed of dialkylfluorene and terpyridine units. In the low-viscosity solvent chloroform, this metallopolymer only exhibits blue emission from the polymeric segment. In contrast, the high-viscosity solvent DMSO induces dual emission: blue emission from the polymer and characteristic red emission of Eu^{3+} [Fig. 11 (A)]. The emission behavior stems from viscosity-induced structural rigidity. High-viscosity environments restricts intramolecular motion and rotation of the polymer backbone and ligand moieties, suppressing non-radiative energy loss and promoting efficient ligand-to-Eu^{3+} energy transfer *via* the antenna effect. The authors subsequently extended this approach to prepare another analogous Tb-containing metallopolymer (**32**) with similar AIE-related properties[51]. Tb^{3+} shows weak emission in low-polarity, low-viscosity solvents. It only displays dual emission (blue for backbone and green for Tb^{3+}) exclusively in high-polarity, high-viscosity DMSO [Fig. 11 (B)][51,52]. These works demonstrate that solvent viscosity regulates the luminescence of lanthanide metallopolymers through motion restriction and conformational control, providing a strategy for tunable dual emission in such hybrid materials.

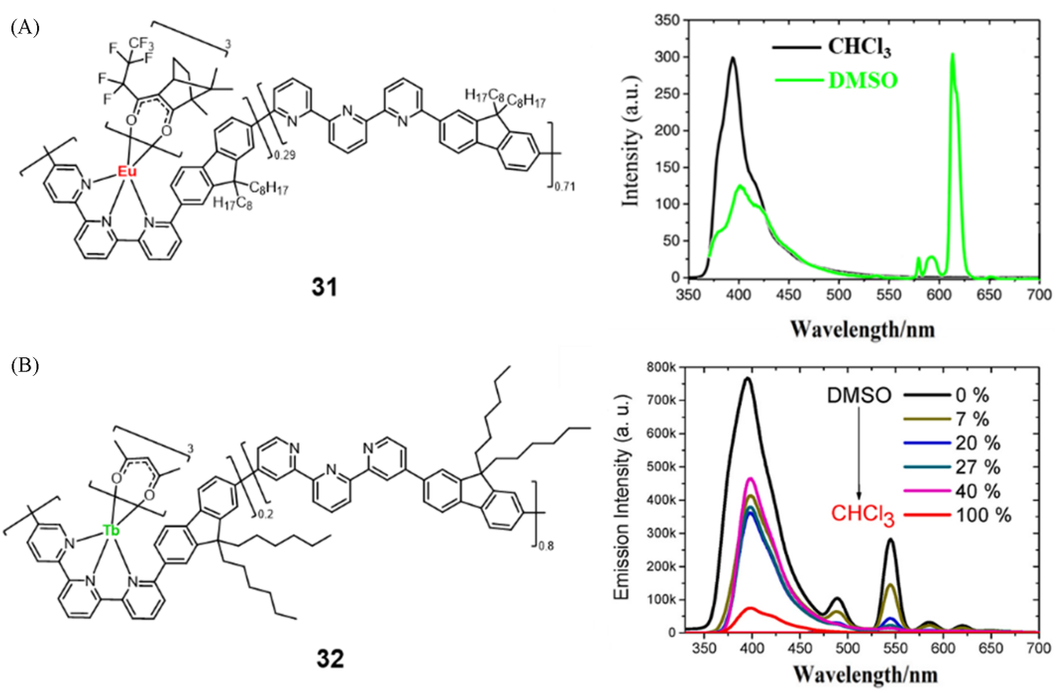

Fig. 11 Molecular structure, PL spectra in chloroform and DMSO of metallopolymer 31(A)[50] and molecular structure of metallopolymer 32 and PL spectra of metallopolymer 32 in DMSO/chloroform mixture with different chloroform fractions(B)[51]

(A) Copyright 2020, Elsevier Ltd.; (B) copyright 2021, Elsevier Ltd.

In addition, there is another type of AIE lanthanide metallopolymers, in which the lanthanide ions only coordinate to pendant side chains of the polymeric backbone. The side chains serve as dedicated coordination loci, while the backbone maintains structural independence. This design preserves the intrinsic flexibility of

backbones and enables precise modulation of the lanthanide coordination environment through side-chain engineering. In some reports, AIEgens are attached to the side chains, which induce the AIE phenomenon in metallopolymers[53—55], while others achieve this without the use of specific AIE units[56—58]. This strategy further enriches the structural diversity and functional tunability of these materials.

A notable example of this strategy that avoids specific AIE units was reported by Zhu *et al.*, who developed a water-soluble Eu^{3+}-containing metallopolymer(**33**) and subsequently extended this approach to a series of dual-lanthanide analogs(**34**) with tunable Eu^{3+}/Tb^{3+} molar ratios[56,57]. Both metallopolymers contain amphiphilic backbones that are formed by free-radical polymerization of polymerizable terpyridine(Tpy) and *N*-(2-hydroxyethyl)acrylamide(HEAA)[Fig.12(A)]. In dilute solutions, these luminescence emit weakly. However, polymer **33** exhibits enhanced characteristic red luminescence upon aggregation because of the RIM of the polymer main chain and the Tpy ligand. Meanwhile, the triplet energy level of Tpy matches the excited state of Eu^{3+}, which optimizes the antenna effect and enables efficient ligand-metal energy transfer. Following this strategy, polymer **34** shows analogous AIE behavior, characterized by weak blue emission from the polymer backbone in dilute solutions and bright white light emission upon aggregation. These works demonstrate the versatility of terpyridine-sensitized lanthanide metallopolymers in modulating AIE.

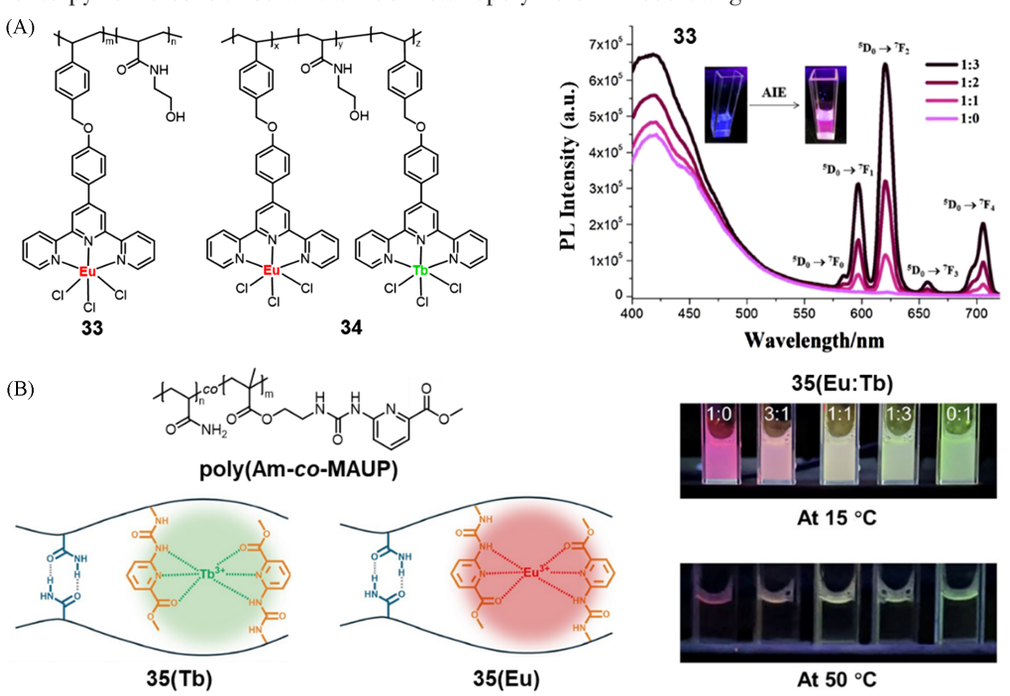

Fig. 12 Molecular structure of polymers 33 and 34 and PL spectra in DMF with different fraction of 1,4-dioxane(A)[56] and molecular structure of poly(Am-*co*-MAUP) and schematic diagram of 35(Tb) and 35(Eu), fluorescent photographs of 35(Ln) consisting of different ratios of Eu^{3+} to Tb^{3+} at 15 ℃ and 50 ℃(B)[58]

(A) Copyright 2018, Elsevier Ltd.; (B) copyright 2025, Science China Press.

Zhao *et al.*[58] developed a series of thermoresponsive metallopolymers [**35**(**Ln**), Ln=Eu, Tb] *via* reversible addition-fragmentation chain transfer(RAFT) copolymerization of acrylamide(Am) and methyl 6-(3-(2-(methacryloyloxy)ethyl)ureido)picolinate(MAUP), where MAUP could coordinate with Ln^{3+} ions [Fig.12(B)]. In aqueous solutions and above the cloud point temperature(T_{cp}), these polymers exhibit relatively weak luminescence. When the temperature drops below T_{cp}, polymer aggregation occurs and endows the materials with enhanced luminescence. The aggregates form a hydrophobic environment that shields Ln^{3+} from water-induced quenching, while the energy levels of the MAUP antenna enable efficient ligand-to-metal energy transfer. This study demonstrates that by altering Eu^{3+}/Tb^{3+} ratios, multicolor emission can be achieved.

2.3.2 Ln^{3+}-Coordination-Induced Emission in Metal Clusters Moving beyond polynuclear systems, the coordination of Ln^{3+} ions with various metal clusters has emerged as another promising AIE platform. These clusters include copper nanoclusters (CuNCs)[59—62], bimetallic nanoclusters (AgCuNCs)[63], and gold nanoclusters (AuNCs)[64—66], where the coordination is driven by carboxyl or thiol groups on cluster-stabilizing ligands. Ln^{3+} ions act as coordination bridges to interact with these surface functional groups, which serve as specific coordination sites and form stable bonds with Ln^{3+} *via* electron-rich oxygen or sulfur atoms. This coordination-driven interaction overcomes electrostatic repulsion between dispersed metal clusters, driving their ordered assembly into compact aggregates. The resulting aggregates effectively restrict intramolecular rotation and vibration of cluster ligands, minimizing non-radiative energy dissipation pathways dominant in the dispersed state. Concurrently, coordination-induced aggregation optimizes energy transfer efficiency between ligands and metal clusters, facilitating efficient energy migration from ligand moieties to metal centers and reducing energy loss during transfer. These synergistic effects give rise to prominent AIE feature, with metal cluster systems transitioning from weakly emissive in the dispersed state to highly luminescent in the aggregate state. The enhanced luminescence features excellent photo-stability and enhanced quantum yields, alongside distinct signal responses to external stimuli. Such systems have been applied in sensing antibiotics, acid/alkaline phosphatase, ATP, phosphate anions, and Cu^{2+} ions, relying on competitive coordination or inner filter effect for signal regulation. Target analytes interact with Ln^{3+} ions or cluster ligands through specific pathways including coordination competition where analytes seize coordination sites due to higher affinity than cluster ligands, electrostatic attraction between complementary charged moieties, or hydrophobic interactions among nonpolar groups. These interactions directly disrupt the original coordination bonds between Ln^{3+} ions and cluster ligands, disassembling the aggregated state of the AIE system into dispersed species. They further hinder efficient energy transfer from cluster ligands to Ln^{3+} ions, interrupting the energy migration pathway and promoting non-radiative decay, thus leading to fluorescence quenching. Chen *et al.*[60] developed a fluorescent probe system based on glutathione-stabilized CuNCs and Tb^{3+} ions, where the coordination of Tb^{3+} induces AIE property. In this work, Tb^{3+} ions coordinate with carboxyl groups of glutathione (the surface ligand of CuNCs), promoting the aggregation of CuNCs (Fig. 13). Such aggregation restricts intramolecular motion and reduces non-radiative energy dissipation, thereby significantly enhancing the luminescence of CuNCs. Notably, 2,6-dipyridyl acid (DPA), a specific biomarker for anthrax spores, exhibits a stronger coordination affinity toward Tb^{3+} than glutathione. This enables DPA to compete for Tb^{3+} and dislodge these ions from the CuNC surface, triggering the dissociation of aggregated CuNCs and subsequent luminescence quenching. This aggregation-

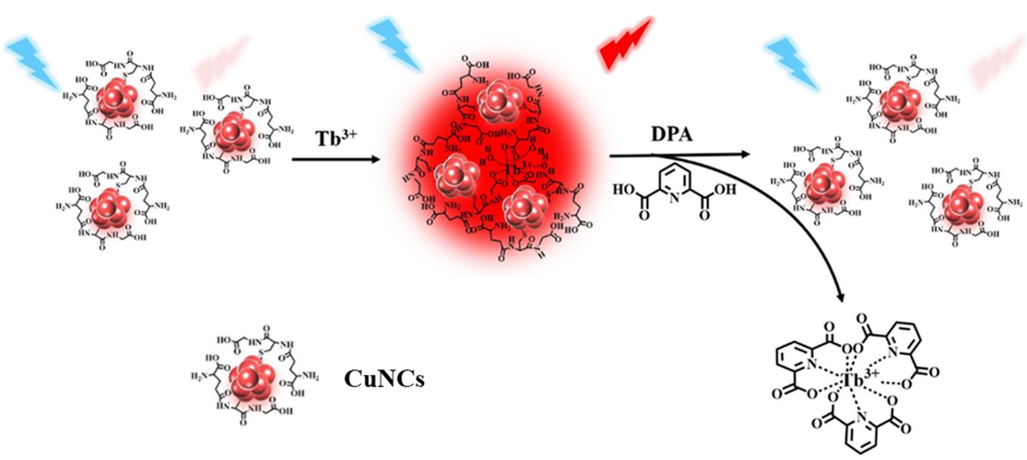

Fig. 13 Schematic diagram of DPA detection based on AIE effect of CuNCs[60]

Copyright 2023, Springer Nature.

dissolution mechanism driven by competitive coordination enables sensitive and selective detection of DPA with a low limit of detection (LOD). Moreover, this system can be applied to the quantitative analysis of real bacterial spores, providing a reliable strategy for monitoring anthrax spore contamination.

2.3.3 Emissive Lanthanide MOFs Metal-organic frameworks (MOFs) are crystalline porous materials formed by coordination interactions between metal ions and organic ligands. They possesses tunable topological structures, morphologies and functions. Emissive lanthanide MOFs have emerged as promising functional materials due to their combined prominent structural and optical properties[67,68]. AIE lanthanide MOFs, constructed by coordinating AIEgens with Ln^{3+}, integrate synergistic and complementary advantages: the intrinsic structural tunability, porous architectures and large specific surface areas of MOFs; the high quantum yield of AIE moieties; as well as the distinctive photophysical characteristics of Ln^{3+}[69]. These combined merits endow them with robust luminescence in the aggregate state and precise modulation of photophysical properties. Consequently, these materials demonstrate superior performance in high-sensitivity and selective chemical sensing[70—77], photobleaching-resistant bioimaging[78], and solid-state lighting[79].

2.4 Summary

To systematically summarize the structural and performance disparities of AIE lanthanide complexes with distinct nuclearity, Table 1 outlines the core characteristics of mononuclear, dinuclear, and polynuclear systems discussed above. It incorporates key information including structural flexibility and representative applications, offering a concise reference for comparing the advantages and limitations of each system. This summary establishes a foundation for the subsequent in-depth analysis of AIE mechanisms and expansion of practical applications.

Table 1 Comparative summary of AIE lanthanide complexes with different number of Ln centers

System type	Structural flexibility	Representative applications
Mononuclear	High	Chemical sensing, bioimaging, and anti-counterfeiting
Dinuclear	Moderate	Solid-state lighting and stimulus-responses
Polynuclear	Low to moderate	Solid-state lighting, chemical sensing, and biosensing

Meanwhile, the photo-physical properties and application orientations of AIE lanthanide complexes are inherently governed by the intrinsic characteristics of Ln^{3+} ions. Table 2 systematically compares the core properties of commonly used Ln^{3+} ions in AIE systems, offering a direct reference for rational ligand design and targeted ion selection in practical applications.

Table 2 Comparative properties of Ln^{3+} ions in AIE lanthanide complexes

Ln^{3+} ion	Emission range (Luminescent color)	Characteristic emission peak/nm	Luminescence lifetime
Tb^{3+}	Visible (Green)	545	ms scale (0.5—2.0 ms)
Eu^{3+}	Visible (Red)	613	ms scale (0.2—1.0 ms)
Sm^{3+}	Visible (Orange)	645	μs scale (1—50 μs)
Yb^{3+}	NIR-II	980	μs scale (1—200 μs)
Nd^{3+}	NIR-II	1064	μs scale (<10 μs)

Together, these two tables list the key information of AIE lanthanide complexes discussed above, providing a clear and intuitive framework for understanding their structural diversity, performance disparities, and design principles, thereby laying a foundation for subsequent mechanistic analysis as well as application development and expansion.

3 Mechanisms of AIE Lanthanide Complexes

From the perspective of energy transfer, the AIE mechanism of lanthanide complexes is distinctly featured by efficient energy transfer from the triplet states of organic ligands to the excited states of Ln^{3+}. This

process is facilitated by the classic antenna effect and closely dependent on well-matched energy level alignment between ligand triplet states and Ln^{3+} excited states (Fig. 14). The complete energy transfer cycle underlying this characteristic behavior proceeds sequentially: organic ligands first absorb external energy and undergo electronic excitation to the singlet excited state (S_1), then experience intersystem crossing (ISC) to populate the triplet excited state (T_1); when the energy level of the ligand T_1 state matches the $4f^*$ excited states of Ln^{3+} in an optimal range, effective energy transfer (ET) occurs from the T_1 state to the $4f^*$ states, followed by the radiative transition of Ln^{3+} ions from the $4f^*$ states back to their ground $4f$ states.

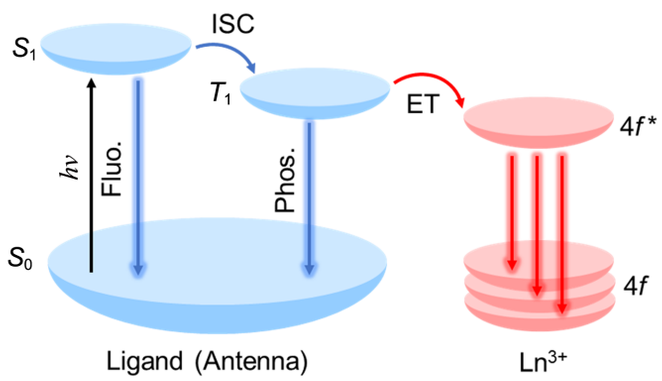

Fig. 14 Energy level diagram illustrating the antenna effect and sequential energy transfer processes for lanthanide complexes with characteristic *f-f* electronic transitions

hν stands for ultraviolet excitation, Fluo. stands for fluorescence, Phos. stands for phosphorescence, ISC stands for intersystem crossing, ET stands for energy transfer, $4f^*$ stands for excited state of Ln^{3+} and $4f$ stands for ground state of Ln^{3+}.

The RIM serves as the dominant AIE mechanism, supplemented by complementary effects contributing to luminescence enhancement upon aggregation. In the dispersed state, flexible moieties within ligands dissipate excited-state energy through non-radiative pathways, resulting in weak luminescence. Changes in environmental pH, solvent polarity, or concentration trigger the aggregation of complexes. This aggregation increases steric hindrance between complexes and enhancement of π-π stacking, thereby restricting the internal movement of the complexes. The aggregate structure forms a hydrophobic protective microenvironment that shields lanthanide centers from external quenchers. Simultaneously, it restricts ligand moiety rotation, enhances molecular rigidity, and strengthens ligand conjugation. These synergistic effects collectively minimize non-radiative decay pathways and enhance efficient radiative emission, thereby boosting the overall luminescence performance of the complexes.

Notably, emerging studies have demonstrated that the AIE feature in certain lanthanide complexes eludes explanation by the classic RIM mechanism. This finding underscores the mechanistic diversity of such systems, a characteristic that sets them apart from organic AIEgens. A representative example involves the unconventional EVD mechanism identified in complex **25**. In dilute aqueous solutions, strong electronic-vibrational coupling between coordinated water molecules and Eu^{3+} induces efficient non-radiative relaxation, resulting in weak luminescence. Increasing the concentration or replacing the solvent with DMF triggers the reorganization of the Eu^{3+} coordination environment and subsequent EVD. This effect reduces resonance between the vibrational energy of coordinating species and Eu^{3+} energy gaps thus suppressing non-radiative decay and enhancing the characteristic emission of Eu^{3+}. Importantly, no colloidal aggregates or nanoparticles are detected even at high concentrations, and luminescence enhancement was not accompanied by restricted intramolecular rotation or vibration of ligand moieties, which clearly deviates from the RIM mechanism.

For metal cluster systems, AIE phenomenon is primarily driven by Ln^{3+}-coordination-induced aggregation. Lanthanide ions coordinate with stable ligands on the cluster surface, thereby inducing aggregation of

clusters. This restricts intramolecular motion of ligand, suppresses non-radiative dissipation, and stabilizes cluster excited states to promote AIE efficiency.

Based on structural constraints and photo-physical regulations during aggregation, the core AIE mechanisms of lanthanide complexes can be systematically classified as follows(Table 3).

Table 3 Summary of core AIE mechanisms in lanthanide complexes

Mechanism	Dominant motion/vibration targeted	Key trigger for AIE
Restriction of intramolecular rotation(RIR)	Intramolecular rotation(flexible moieties)	Aggregation-induced steric hindrance/intermolecular interactions
Restriction of intramolecular vibration(RIV)	Intramolecular vibration(ligand backbones)	Aggregation-induced conformational rigidity
Electronic-vibrational decoupling(EVD)	Electronic-vibrational coupling	Concentration increase/solvent-induced ligand exchange
Ln^{3+}-coordination-induced aggregation	Cluster dispersion-aggregation transition	Ln^{3+}-ligand coordination

(1) Restriction of intramolecular rotation(RIR). As the most prevalent mechanism, RIR governs nearly all mononuclear complexes with AIE-active ligands and most polynuclear metallopolymers. It relies on aggregation-induced steric hindrance and intermolecular interactions to suppress the free rotation of flexible ligand moieties, minimizing non-radiative energy dissipation and facilitating ligand-to-Ln^{3+} energy transfer.

(2) Restriction of intramolecular vibration(RIV). RIV is a specialized mechanism observed in complexes with ligands bearing high-frequency vibrational units, such as pinacol ligands in dinuclear complex **27**. Unlike RIR, which targets rotational motion, RIV restricts intramolecular vibration of ligand backbones or functional groups upon aggregation, reducing vibrational coupling between ligands and Ln^{3+} ions and further enhancing radiative emission. It often acts as a complementary mechanism to RIR but can be dominant in systems with rigid rotational moieties yet flexible vibrational units.

(3) Electronic-vibrational decoupling(EVD). EVD represents an unconventional mechanism unrelated to molecular motion restriction, exclusively reported in specific mononuclear complexes such as complex **25**. It is triggered by the reorganization of the coordination environment upon concentration elevation or solvent switching. This reorganization reduces the resonance between solvent/ligand vibrational energies and Ln^{3+} electronic energy gaps, suppressing non-radiative relaxation without the formation of colloidal aggregates.

(4) Ln^{3+}-coordination-induced aggregation. Ln^{3+}-coordination-induced aggregation is a unique mechanism specific to metal cluster systems. In these systems, Ln^{3+} ions coordinate with cluster-stabilizing ligands to drive cluster aggregation, which restricts ligand motion and stabilizes the excited states of the clusters.

The AIE property of lanthanide complexes originates from synergistic structural and photophysical modifications during aggregation. These modifications collectively suppress non-radiative decay and optimize the ligand-to-metal energy transfer. Understanding these mechanisms provides valuable guidance for rational material design.

4 Applications of AIE Lanthanide Complexes

4.1 Stimuli Responses

Organic AIE materials offer distinct advantages in stimulus-responsive applications[80]. AIE lanthanide complexes further integrate these merits with the unique optical properties of Ln^{3+}, affording advanced stimulus-responsive luminescent systems.

Notably, a representative example of such advanced stimulus-responsive AIE lanthanide complexes is the dynamic chiral Eu^{3+} complexes[**17**(**R**), **17**(**S**) and **18**(**R**), **18**(**S**)] reported by Zou *et al.*, which exhibit

highly sensitive and selective responses to Cu^{2+} ions[Fig.15(A)][33]. These complexes exhibit significant luminescence quenching effect upon interaction with Cu^{2+} ions, with LOD as low as 2.55 nmol/L[for **17**(**R**)] and 4.44 nmol/L[for **18**(**R**)], far below the 20 μmol/L maximum permissible concentration for drinking water stipulated by the U. S. Environmental Protection Agency(USEPA). The sensing mechanism involves Cu^{2+} ions displacing Eu^{3+} in the complex structure, triggering strong LMCT that quenches the characteristic Eu^{3+} emission. Notably, the complexes maintain high selectivity for Cu^{2+} ions even in the presence of multiple interfering metal ions including Co^{2+}, Fe^{3+}, Ag^{+} and Ca^{2+}. They also exhibit reliable performance across a range of pH value from 4 to 11, with LOD as low as 0.081 nmol/L under acidic conditions. Furthermore, their fast and efficient luminescence quenching response to Cu^{2+} ions facilitates dual anti-counterfeiting applications when formulated into inks, enabling visible pattern encryption under UV irradiation.

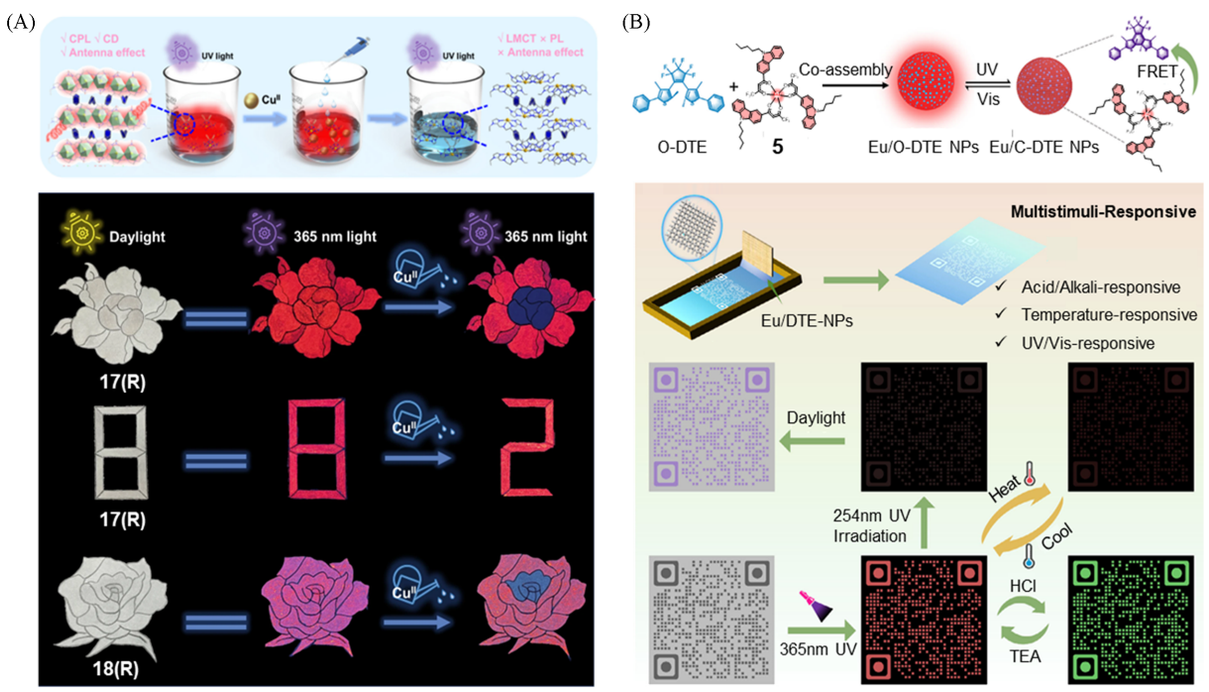

Fig. 15 Schematic diagram of the response mechanism of the complexes 17(R, S) and 18(R, S) to copper ions and its real applications(A)[33] and schematic illustration of 5 NPs assemblies and Eu/DTE-NPs co-assemblies and application of Eu/DTE-NPs in multidimensional dynamic information encryption(B)[25]

(A) Copyright 2024, Springer Nature; (B) copyright 2025, John Wiley and Sons.

Beyond the Cu^{2+}-responsive AIE lanthanide complexes reported by Zou *et al.*[33], Tang *et al.*[25] developed Eu/DTE-NPs with versatile applications in advanced information security[Fig.15(B)]. Eu/DTE-NPs, fabricated by co-assembling of complex **5** and *o*-dithienylethene(*o*-DTE), exhibit multi-stimuli responsiveness toward pH value, temperature, and UV/Vis light. These nanoparticles enable multiple stimuli-responsive information encryption, featuring pH-triggered reversible red-to-green fluorescence switching, temperature-modulated luminescence ON/OFF cycling, and UV/Vis light-controlled Förster resonance energy transfer(FRET) for precise emission regulation. These nanoparticles can be made into various encryption tools, including screen-printed QR codes and specialized hydrogels. These hydrogels maintain reversible light-responsive property switching. Sequential application of appropriate stimuli allows these tools to reveal hidden information. Additionally, leveraging the inherent randomness of nanoparticle assembly, Eu/DTE-NPs can serve as physical unclonable functions(PUFs) with luminescence intensity and lifetime dual cryptographic keys, achieving ultrahigh encoding capacity of 4^{1600} and excellent stability against thermal and optical stresses. This provides a robust strategy for unforgeable authentication and dynamic anti-counterfeiting.

4.2 Biological Imaging

AIE lanthanide complexes offer unique advantages for bioimaging, including resistance to ACQ for stable luminescence in high-concentration biological environments, narrow emission bands that minimize autofluorescence interference, long luminescence lifetimes enabling time-gated detection to eliminate background noise, and excellent biocompatibility that reduces *in vivo* toxicity. These characteristics overcome critical challenges in traditional fluorescent imaging, such as weak signal intensity and poor tissue penetration.

A notable illustration of these superior bioimaging capabilities is provided by Zhu *et al.*, who developed a pair of chiral Eu^{3+} complexes[**19**(**R**) and **19**(**S**)] for high-performance bioimaging, particularly focusing on *in vivo* zebrafish imaging[Fig. 16(A)][35]. When incubated post-fertilization zebrafish embryos for 48 h and 3-day-old larvae at 50 μg/mL for 1—12 h, both complexes are efficiently absorbed, exhibiting gradually intensified red luminescence with incubation time and specifically labeling the yolk sac, intestine, and liver. Beyond zebrafish imaging, the complexes also enable high-resolution lysosomal labeling in human cells such as HeLa and MCF-7 cells, highlighting their versatile potential in biomedical research.

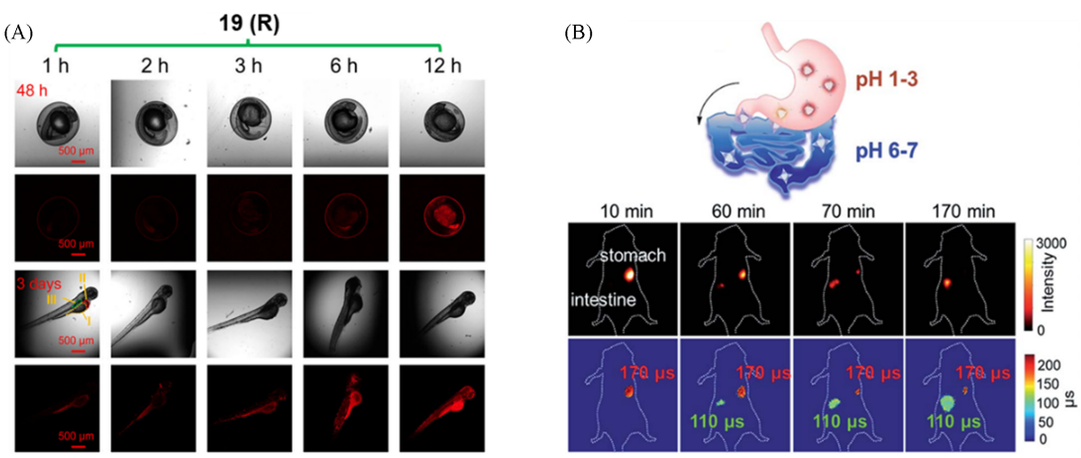

Fig. 16 CLSM images and fluorescence intensity diagrams of zebrafish embryos(48 h after fertilization) and larvae (day 3) after incubation with complex 19(R)(A)[35] and schematic illustration of the metabolic process of complex 22 from the stomach to the intestine, and NIR fluorescence intensity imaging of complex 22(B)[37]

(A) Copyright 2025, Springer Nature; (B) copyright 2019, the Royal Society of Chemistry.

Another notable advance in AIE lanthanide complex-based bioimaging and *in vivo* monitoring comes from Zhang *et al.*, who developed a Yb(III)-based NIR probe(**22**) for non-invasive gastrointestinal pH monitoring with time-dependent tissue distribution and response characteristics[Fig. 16(B)][37]. After oral gavage in mice, the probe initially localizes in the stomach within the first 10 min. It exhibits intense NIR emission and a long lifetime(*ca.* 170 μs), which corresponds to the acidic gastric environment(pH≈1.5). As gastric emptying proceeds, the luminescence signal in the stomach gradually diminishes, while that in the intestine increases. By 170 min, the luminescence signal in the stomach nearly disappears, and the intestine retains a shorter lifetime(*ca.* 110 μs) matching its neutral environment(pH≈6.0). Such versatile capabilities underscore the potential of the probe in gastrointestinal diagnostics and therapeutics.

5 Conclusions and Outlook

AIE lanthanide complexes, featuring varied architectures and distinct luminescent behaviors, have gained extensive applications in diverse fields. This review provides a comprehensive overview of AIE lanthanide complexes by dividing into mononuclear, dinuclear, polynuclear, and lanthanide-ion-coordinated metal cluster architectures. These complexes combine the inherent merits of Ln^{3+} with the AIE feature, enabling

diverse applications in stimulus-responsive detection, advanced information security, and high-resolution biological imaging.

Nonetheless, the development of AIE lanthanide complexes still faces several unresolved challenges that require further exploration. First, compared with organic AIE molecules and transition metal complexes, AIE lanthanide complexes hold great potential for advancement, particularly in mechanistic research. The exploration of AIE mechanism in lanthanide complexes lags behind that in organic compounds and transition metal complexes, with most interpretations relying on the mechanisms of organic AIEgens. However, lanthanide complex systems are notably complicated and variable, and no universally accepted mechanism has been established to explain all cases.

Second, research on lanthanide metallopolymers needs further advancement. Compared with small molecule complexes, metallopolymers possess higher molecular weights and more diverse structural tunabilities. However, their low solubility limits their further applications. Therefore, the issue of polymer solubility should be given sufficient attention. Additionally, investigating the AIE mechanism of metallopolymers should focus on their distinct aggregation behaviors compared to small molecules.

Third, the aggregation behaviors of AIE lanthanide complexes require in-depth exploration. Specifically, the effects of solvent viscosity changes, concentration variations, and stimulus-responsive factors on molecular properties demand systematic investigation. Aggregation behaviors induced by environmental fluctuations are critical for clarifying the underlying AIE mechanisms.

Fourth, the application scope of AIE lanthanide complexes can be further expanded. The unique properties of AIE lanthanide complexes, such as narrow emission, long lifetime and larger Stokes shift, are crucial for expanding their applications. Therefore, exploring the potential value of lanthanide ions is another important direction. For instance, the strong X-ray absorption ability of Ln^{3+} endows AIE lanthanide complexes with great potential for application in X-ray scintillators.

By addressing these existing challenges through structural innovation, mechanistic deepening, and application-oriented optimization, future research will unlock the full potential of AIE lanthanide complexes, promoting their integration into practical technologies ranging from advanced sensors to next-generation optoelectronics and biomedical devices.

References

[1] Luo J., Xie Z., Lam J. W. Y., Cheng L., Chen H., Qiu C., Kwok H. S., Zhan X., Liu Y., Zhu D., Tang B. Z., *Chem. Commun.*, **2001**, (18), 1740—1741
[2] Han P. B., Xia E. H., Qin A. J., Tang B. Z., *Coord. Chem. Rev.*, **2022**, *473*, 214843
[3] Yang S. Y., Zhang L., Kong F. C., Chen Y. Y., Li W. J., Wang F., Liu C., He X., Xiao X. D., Wang J., Sun J. W., Chow P. C. Y., Kwok R. T. K., Lam J. W. Y., Tang B. Z., *Chem*, **2025**, *11*(5), 102534
[4] Yan D., Wang D., Tang B. Z., *Nat. Rev. Bioeng.*, **2025**, *3*(11), 976—991
[5] Chen W. Z., Guan H. T., Lu Y. F., Zeng G. H., Gu D., Guo K. Y., Jiang C., Liu H. X., *Aggregate*, **2025**, *6*(4), e70008
[6] Mei J., Hong Y. N., Lam J. W. Y., Qin A. J., Tang Y. H., Tang B. Z., *Adv. Mater.*, **2014**, *26*(31), 5429—5479
[7] Mei J., Leung N. L. C., Kwok R. T. K., Lam J. W. Y., Tang B. Z., *Chem. Rev.*, **2015**, *115*(21), 11718—11940
[8] Yang S. Y., Chen Y. Y., Kwok R. T. K., Lam J. W. Y., Tang B. Z., *Chem. Soc. Rev.*, **2024**, *53*(11), 5366—5393
[9] Pei Y., Sun Y., Huang M. J., Zhang Z. J., Yan D. Y., Cui J., Zhu D. X., Zeng Z. B., Wang D., Tang B. Z., *Biosensors*, **2022**, *12*(12), 1104
[10] Mauro M., Cebrián C., *Isr. J. Chem.*, **2018**, *58*(8), 901—914
[11] Sathish V., Ramdass A., Thanasekaran P., Lu K. L., Rajagopal S., *J. Photoch. Photobio. C*, **2015**, *23*, 25—44
[12] Wang F., Liu X. G., *Chem. Soc. Rev.*, **2009**, *38*(4), 976—989
[13] Furet E., Costuas K., Rabiller P., Maury O., *J. Am. Chem. Soc.*, **2008**, *130*(7), 2180—2183
[14] Thibon A., Pierre V. C., *Anal. Bioanal. Chem.*, **2009**, *394*(1), 107—120
[15] Wang T., Wang S. F., Liu Z. Y., He Z. Y., Yu P., Zhao M. Y., Zhang H. X., Lu L. F., Wang Z. X., Wang Z. Y., Zhang W. A., Fan Y., Sun C. X., Zhao D. Y., Liu W. M., Bünzli J. C. G., Zhang F., *Nat. Mater.*, **2021**, *20*(11), 1571—1578

[16] Xu J., Luo R., Luo Z. C., Xu J., Mu Z., Bian H. Y., Chan S., Y., Tan. B. Y. H., Chi D. Z., An Z. F., Xing G. C., Qin X., Gong C. Y., Wu Y. M., Liu X. G., *Nat. Photon.*, **2025**, *19*(1), 71—78
[17] Andres J., Hersch R. D., Moser J. E., Chauvin A. S., *Adv. Funct. Mater.*, **2014**, *24*(32), 5029—5036
[18] Yang Y. L., Hu X. M., Yang Z., Huang W., *Adv. Funct. Mater.*, **2025**, *35*(2), 2412970
[19] Fernández-Fariña S., Kotova O., Donohoea S. R., Gunnlaugsson T., *Chem. Soc. Rev.*, **2025**, *54*(23), 11226—11265
[20] Zhang Y., Jiao P. C., Xu H. B., Tang M. J., Yang X. P., Huang S. M., Deng J. G., *Sci. Rep.*, **2015**, *5*(1), 9335
[21] Wu J. J., Zhao C., Zhu Z. H., Li X. L., Ashebr T. G., Tang J. K., *Chem. Asian J.*, **2022**, *17*(23), e202200913
[22] Zhuo H., Guan D. B., He J. C., Xu H. B., Zeng M. H., *Chem. Eur. J.*, **2021**, *27*(65), 16204—16211
[23] Su P. R., Liang L. J., Wang T., Zhou P. P., Cao J., Liu W. S., Tang Y., *Chem. Eng. J.*, **2021**, *413*, 127408
[24] Wang S. Y., Wang L., Fang F., Ma X., Guo Y. Y., Wang R. D., Zhang S. S., Zhang Z., Du L., Zhao Q. H., *Inorg. Chem. Front.*, **2023**, *10*(18), 5258—5269
[25] Liang L. J., Yang X., Yan X. Y., Kou Y., Zhang Y. H., Su P. R., Tang Y., *Adv. Mater.*, **2026**, *38*(2), e14252
[26] de Sá G. F., Malta O. L., de Mello-Donegá C., Simas A. M., Longo R. L., Santa-Cruz P. A., da Silva E. F. Jr., *Coord. Chem. Rev.*, **2000**, *196*(1), 165—195
[27] Kai T., Kishimoto M., Akita M., Yoshizawa M., *Chem. Commun.*, **2018**, *54*(8), 956—959
[28] Xu M. J., Wang J. H., Liao Z. X., Liu J. Q., Yi H., Hao H. X., Li F., Xu S. Y., Liu F. F., Peng Y. L., Wang S. L., Cao X. D., Zhang P. F., *Luminescence*, **2025**, *40*(8), e70289
[29] Wong H. Y., Chan W. T. K., Law G. L., *Molecules*, **2019**, *24*(4), 662
[30] Su P. R., Wang T., Zhou P. P., Yang X. X., Feng X. X., Zhang M. N., Liang L. J., Tang Y., Yan C. H., *Natl. Sci. Rev.*, **2022**, *9*(1), nwab016
[31] Chen F. F., Wang J. M., Xu W., Ren Z. Z., Peng G., Huang T., Zhao F., *J. Alloy. Compd.*, **2025**, *1010*, 177421
[32] Zhang G. P., Zhu H. X., Chen M. J., Pietraszkiewicz M., Pietraszkiewicz O., Li H. G., Hao J. C., *Chem. Eur. J.*, **2018**, *24*(59), 15912—15920
[33] Li Y. L. Wang H. L., Zhu Z. H., Wang Y. F., Liang F. P., Zou H. H., *Nat. Commun.*, **2024**, *15*(1), 2896
[34] Wang H. L., Yu B., Liang F. P., Zou H. H., *Chin. Chem. Lett.*, **2025**, 111346
[35] Qin W. W., Yu B., Zhang G. H., Tang M. J., Zou H. H., Liang F. P., Zhu Z. H., *Rare Met.*, **2025**, *44*(12), 10390—10403
[36] Yang S. S., Guo Z. P., Hu Z. Q., Guo D. C., *Luminescence*, **2021**, *36*(2), 306—315
[37] Ning Y. Y., Cheng S. M., Wang J. X., Liu Y. W., Feng W., Li F. Y., Zhang J. L., *Chem. Sci.*, **2019**, *10*(15), 4227—4235
[38] Bodedla G. B., Zhu X., Wong W. Y., *Aggregate*, **2023**, *4*(3), e330
[39] Wang Y. F., Wang J. J., Zhang S. W., Tang N., Ou X. W., Jiang J. H., Ma F. L., Alam P., Qiu Z. J., Wang W. J., Zhao Z., Lam J. W. Y., Tang B. Z., *ACS Nano*, **2025**, *19*(27), 25042—25051
[40] Leng J. Q., Li H. F., Chen P., Sun W. B., Gao T., Yan P. F., *Dalton Trans.*, **2014**, *43*(32), 12228—12235
[41] Ai J. F., Li Y. L., Wang H. L., Liang F. P., Zhu Z. H., Zou H. H., *Inorg. Chem.*, **2023**, *62*(48), 19552—19564
[42] Nakai T., Shima K., Shoji S., Fushimi K., Hasegawa Y., Kitagawa Y., *Front. Chem.*, **2023**, *11*, 1154012
[43] Pan J. K., Chen Z., Wang H., Li X. P., Yu X. J., *Sci. China Mater.*, **2025**, *68*(10), 3485—3510
[44] Yang D. Q., Li H. M., Li H. R., *Coord. Chem. Rev.*, **2024**, *514*, 215875
[45] Zhu Y. X., Wei Z. W., Pan M., Wang H. P., Zhang J. Y., Su C. Y., *Dalton Trans.*, **2016**, *45*(3), 943—950
[46] Raghuvanshi K., Verma A., Sunkari S. S., *J. Lumin.*, **2025**, *283*, 121284
[47] Tong Y. J., Yu L. D., Wu L. L., Cao S. P., Zhang L., Xia X. H., Qiu J. D., *Chem. Commun.*, **2018**, *54*(54), 7487—7490
[48] Tong Y. J., Song A. M., Yu L. D., Liang R. P., Qiu J. D., *Microchim. Acta*, **2019**, *187*(1), 53
[49] Qi W. J., Zhao M. Y., Fu Y. L., He H. K., Tian X., Wu D., Zhang Y., Hu P. P., *Dyes Pigm.*, **2020**, *172*, 107797
[50] Campos E. C. G., Turchetti D. A., Santana A. J., Domingues R. A., Duarte L., Atvars T. D. Z., Akcelrud L., *Synth. Met.*, **2021**, *273*, 116686
[51] Campos E. C. G., Turchetti D. A., Zanlorenzi C., Domingues R. A, Duarte L. G. T. A., Atvars T. D. Z., Akcelrud L., *Polymer*, **2021**, *229*, 123990
[52] Campos E. C. G., Turchetti D. A., Domingues R. A., Akcelrud L. C., *Synth. Met.*, **2025**, *311*, 117802
[53] Zhang S. X., Yin W. D., Yang Z. M., Shah I., Yang Y., Li Z., Zhang S. J., Zhang B., Lei Z. Q., Ma H. C., *Anal. Chem.*, **2020**, *92*(1), 7808—7815
[54] Huang Y. J., Feng W. X., Zhou Z. P., Zheng H. Z., Zhao Y., Yan H. X., Lv X. Q., *J. Mater. Chem. C*, **2022**, *10*(19), 7586—7593
[55] Feng W. X., Huang Y. J., Zhao Y., Tian W., Yan H. X., *ACS Appl. Mater. Interfaces*, **2023**, *15*(13), 17211—17221
[56] Zhang Z., Chang H., Kang Y. F., Li X. P., Jiang H. E., Xue B. L., Wang Y. Y., Lv X. Q., Zhu X. J., *Sensor. Actuat. B-Chem.*, **2019**, *282*, 999—1007
[57] Zhang Z., Chen Y. X., Chang H., Wang Y. Y., Li X. P., Zhu X. J., *J. Mater. Chem. C*, **2020**, *8*(6), 2205—2210
[58] Fan X. Z., Zhou Z. H., Luo M. Q., Banquy X., Zhang J. W., Zhu X. X., Zhang C. Z., *Sci. China Chem.*, **2025**, *68*(11), 5949—5959
[59] You J. G., Lu C. Y., Kumar A. S. K., Tseng W. L., *Nanoscale*, **2018**, *10*(37), 17691—17698
[60] Ma F. H., Deng L., Wang T. T., Zhang A. M., Yang M. H., Li X. Q., Chen X., *Microchim. Acta*, **2023**, *190*(8), 291

[61] Ma J., Cong X., Ou K. D., Liao Y. G., Yang Y. J., Wang H., *Sensor. Actuat. B-Chem.*, **2023**, *390*, 133904
[62] Huang X. M., Chen H. Y., Huang R., Shi Y. D., Ye R. H., Qiu B., *Microchim. Acta*, **2024**, *191*(1), 54
[63] Mu J., Zhang H. F., Huang Z. Z., Jia Q., *Spectrochim. Acta A*, **2023**, *291*, 122388
[64] Pan T. T., Zhou T., Tu Y. F., Yan J. L., *Talanta*, **2021**, *227*, 122197
[65] Miao W. J., Wang L., Liu Q., Guo S., Zhao L. Z., Peng J. J., *Chem. Asian J.*, **2021**, *16*(3), 247—251
[66] Madni A., Zhang Y. C., Zhang L. Y., Qiang Y. N., Qi S. D., Zhai H. L., *Food Compos. Anal.*, **2025**, *148*, 108429—
[67] Saraci F., Quezada-Novoa V., Donnarumma P. R., Howarth A. J., *Chem. Soc. Rev.*, **2020**, *49*(22), 7949—7977
[68] Xu H., Cheng P., *Aggregate*, **2024**, *5*(3), e518
[69] Yin H. Q., Wang X. Y., Yin X. B., *J. Am. Chem. Soc.*, **2019**, *141*(38), 15166—15173
[70] Yang L., Dou Y., Qin L., Chen L. L., Xu M. Z., Kong C., Zhang D. P., Zhou Z., Wang S. N., *Inorg. Chem.*, **2020**, *59*(22), 16644—16653
[71] Li G. Y., Tong C. L., *Anal. Chim. Acta*, **2020**, *1133*, 11—19
[72] Li Z. J., Jiang F. L., Yu M. X., Li S. C., Chen L., Hong M. C., *Nat. Commun.*, **2022**, *13*(1), 2142
[73] Xu S. J., Xiong G., Zhang X. Y., Huang K., Qin D. B., Zhao B., *Cryst. Growth Des.*, **2023**, *23*(6), 4214—4221
[74] Zhai X. Y., Kou Y., Liang L. J., Liang P. Y., Su P. R., Tang Y., *Inorg. Chem.*, **2023**, *62*(45), 18533—18542
[75] Yan Z. W., Ling Y., Zeng Q., Sun Z., Li N. B., Luo H. Q., *Sensor. Actuat. B-Chem.*, **2024**, *417*, 136169
[76] Li Y. L., Wang H. L., Xiao Z. X., Ai J. F., Liang F. P., Zhu Z. H., Zou H. H., *ACS Appl. Mater. Interfaces*, **2024**, *16*(45), 62301—62313
[77] Wang H. L., Li Y. H., Zou H. H., Liang F. P., Zhu Z. H., *Adv. Mater.*, **2025**, *37*(29), 2502742
[78] Li Z. J., Zhang J. P., Wu Z. Y., Lei H., Zhao Y. F., Qi W. Q., Gao X., Jiang F. L., Liu Y. S., Chen L., Hong M. C., *Adv. Sci.*, **2025**, *12*(4), e10147
[79] Li X. Q., Zhao J. W., Wang Y. L., Liu W., Zhao S. S., Chen X., Tian T. Y., Zhang H., Sun Q., Zhao Z., *Inorg. Chem.*, **2025**, *64*(34), 17313—17321
[80] Zhang J., He B. Z., Hu Y. P., Alam P., Zhang H. K., Lam J. W. Y., Tang B. Z., *Adv. Mater.*, **2021**, *33*(32), 2008071

(Ed.: H, K, M)